

ORIGINAL RESEARCH



Tbc1d10c is a selective, constitutive suppressor of the CD8 T-cell anti-tumor response

Adrienne O. Cohen^a, Seung-Hyun Woo^{a,b}, Junya Zhang^a, Jiyeon Cho^{a,c}, Marlon E. Ruiz^{a,d}, Jianli Gong^{a,e}, Rong Du^a, Olga Yarygina^a, Danya Z. Jafri^a, Michael A. Bachelor^{a,f}, Michael O. Finlayson^{g,h}, Rajesh K. Soniⁱ, Matthew S. Hayden^j, and David M. Owens^{b,a,k}

^aDepartment of Dermatology, Columbia University Irving Medical Center, Vagelos College of Physicians & Surgeons, New York, NY 10032, USA; ^bDiscovery Biology Division, Velia Therapeutics, San Diego, CA, USA; ^cGlobal Safety Assurance, Reckitt Benckiser Inc., Montvale, NJ, USA; ^dOlink Proteomics, Los Angeles, CA 90045, USA; ^eProcessing Cell Sciences, Merck & Co., Inc, Kenilworth, NJ, USA; ^fBoston Scientific, Center for Biological Innovation, Global Preclinical Sciences, Marlborough, MA, USA; ^gDepartment of Systems Biology, Columbia University Irving Medical Center, Vagelos College of Physicians & Surgeons, New York, NY, USA; ^hSimons Foundation, New York, NY 10010, USA; ⁱProteomics & Macromolecular Crystallography Shared Resource, Herbert Irving Comprehensive Cancer Center, Columbia University Irving Medical Center, New York, NY 10032, USA; ^jDepartment of Surgery, Geisel School of Medicine, Dartmouth College, Hanover, NH, USA; ^kDepartment of Pathology & Cell Biology, Columbia University Irving Medical Center, Vagelos College of Physicians & Surgeons, New York, NY, USA

ABSTRACT

Cancer immunotherapy approaches target signaling pathways that are highly synonymous between CD4 and CD8 T-cell subsets and, therefore, often stimulate nonspecific lymphocyte activation, resulting in cytotoxicity to otherwise healthy tissue. The goal of our study was to identify intrinsic modulators of basic T lymphocyte activation pathways that could discriminately bolster CD8 anti-tumor effector responses. Using a *Tbc1d10c* null mouse, we observed marked resistance to a range of tumor types conferred by *Tbc1d10c* deficiency. Moreover, tumor-bearing *Tbc1d10c* null mice receiving PD-1 or CTLA-4 monotherapy exhibited a 33% or 90% cure rate, respectively. While *Tbc1d10c* was not expressed in solid tumor cells, *Tbc1d10c* disruption selectively augmented CD8 T-cell activation and cytotoxic effector responses and adoptive transfer of CD8 T cells alone was sufficient to recapitulate *Tbc1d10c* null tumor resistance. Mechanistically, *Tbc1d10c* suppressed CD8 T-cell activation and anti-tumor function by intersecting canonical NF- κ B pathway activation via regulation of Map3k3-mediated IKK β phosphorylation. Strikingly, none of these cellular or molecular perturbations in the NF- κ B pathway were featured in *Tbc1d10c* null CD4 T cells. Our findings identify a *Tbc1d10c*-Map3k3-NF- κ B signaling axis as a viable therapeutic target to promote CD8 T-cell anti-tumor immunity while circumventing CD4 T cell-associated cytotoxicity and NF- κ B activation in tumor cells.

ARTICLE HISTORY

Received 25 February 2022
Revised 21 October 2022
Accepted 25 October 2022

KEYWORDS

Immuno-oncology;
squamous cell carcinoma;
melanoma; carabin; NF- κ B;
Map3k3

Introduction

The presence of activated cytotoxic (CD8) T cells within the tumor microenvironment is critical for the eradication of cancer.¹ Yet, many tumors circumvent cytotoxic T-cell elimination through mechanisms such as the reduction of tumor antigen expression, the presentation of molecules that engage immune checkpoints (e.g. PD/L-1, CTLA-4), or the secretion of immunoregulatory molecules.^{2–4} Indeed, some of the most impactful cancer treatments are immunotherapies that counteract these immunosuppressive actions, such as CTLA-4 and PD-1/PDL-1 checkpoint inhibitor antibodies, Chimeric Antigen Receptor (CAR)-T-cell therapy, or adoptive transfer of tumor infiltrating lymphocytes (TILs).^{5–8} However, these therapies can cause severe toxicity or autoreactivity in patients,^{9,10} and they are not yet optimal or efficacious for many patients,^{2,5,6,8,10} necessitating novel therapies to target cancerous malignancies while sparing healthy tissues.

Current FDA-approved immunotherapies designed to increase T-cell effector function target proteins or pathways that are typically present in both CD4 and CD8 T cells. CTLA-4 or PD-1 checkpoint blockade therapies, for instance,

stimulate intra-tumoral cytotoxic effector activity but can also stimulate effector autoreactivity in otherwise healthy tissues. As a result, immunotherapy treatments often carry undesirable side effects such as diarrhea, rash, pruritis, colitis, myocarditis, hepatitis, nephritis, encephalitis, thyroiditis, and pneumonitis.^{10–12} These adverse reactions can occur in up to 60% of patients on CTLA-4 monotherapy treatment, with 10–30% of these cases being potentially fatal.^{11,13,14} Likewise, PD-1/PDL-1 monotherapy demonstrates a substantial side effect profile that includes fatigue, headache, and nausea as well as similar inflammatory disorders mentioned above,^{11,15,16} although PDL-1 therapy appears to be less toxic than PD-1 therapy,¹⁷ these side effects occur in 5–20% of patients, with serious adverse reactions in up to 10% of patients.¹¹ Combination therapy demonstrates a higher degree of side effects and more commonly leads to treatment discontinuation.^{11,18} Likewise, CAR-T-cell therapy is associated with neurological toxicity, including headaches, seizures, or loss of consciousness, as well as allergic reactions, increased risk of serious infections, low blood cell counts, and cytokine release syndrome (CRS).^{10,19,20} A recently developed CAR

called Hu19-CD828Z that targets the CD19 receptor shows a dramatic reduction of neurological toxicity and CRS from 50% to 5% of patients.²¹ In some cases, adverse reactions can be tolerated with the administration of over-the-counter pain medications, lose-dose steroids, or immunosuppressants.¹¹ However, more severe cases require treatment discontinuation or prove fatal to the patient.^{10,11} As such, the aforementioned clinical phenomena underscore the need for efficacious immunotherapies that target activation pathways selective for CD8 T cells to augment anti-tumor cytotoxic function without impacting CD4 T-cell subsets in healthy tissue, including Th1 or regulatory T cells (Tregs) that inhibit autoreactivity. However, a major impediment to fulfilling this need is that the majority of signaling proteins involved in T-cell activation, such as the canonical T-cell receptor signaling pathway, are largely synonymous between CD4 and CD8 T-cell subsets.^{22–24}

TBC1D10C has been shown to play an immunosuppressive role in human CD4 T-cell activation²⁵ and murine B-cell-mediated autoimmunity.²⁶ These previous findings suggest that TBC1D10C function may play a role in a variety of disease states involving perturbed lymphocyte activation such as cancer. Indeed, previous metadata analyses across multiple cancer types^{27–31} suggest that *TBC1D10C* expression may be relevant for tumorigenesis. However, any functional role for TBC1D10C in the immune response to cancer has not been reported. Our work demonstrates that genetic disruption of *Tbc1d10c*, also referred to as *Carabin*, selectively confers increased CD8 T-cell-mediated anti-tumor immunity responses with little to no impact on CD4 T cell levels or activation status. Mechanistically, augmented CD8 T-cell activation and cytotoxic function conferred by *Tbc1d10c* deficiency was due to increased Map3k3 protein stability, which intersects the NF- κ B pathway via activation of the IKK complex in untouched and TCR ligated CD8 T cells. However, no perturbations in canonical NF- κ B pathway proteins were observed in *Tbc1d10c*-deficient CD4 T cells. As such, our findings identify a *Tbc1d10c*-Map3k3 intersection with the canonical NF- κ B pathway as a selective therapeutic target to promote anti-tumor immune responses that may also circumvent undesirable cytotoxicity.

Materials and Methods

Animals

The targeting cassettes for *Tbc1d10c* null (*Tbc1d10c*^{-/-}) and *Tbc1d10c*-*CreER*^{T2} transgenic mice were generated in our laboratory by bacterial artificial chromosome (BAC) recombination approaches,³² and chimeric and transgenic founder mice were generated by the CUIMC Transgenic Mouse Core Facility (Supplemental Figures S1 and S2). Experimental *Tbc1d10c*^{-/-} and *Tbc1d10c*^{+/+} (wild-type) mice were generated by backcrossing ten generations onto C57Bl/6 and FVB genetic backgrounds. *Tbc1d10c*-*CreER*^{T2} mice, backcrossed ten generations onto a FVB background, were crossed with FVB-backcrossed *Rosa26*^{mT/mG} mice³³ (Jackson Laboratories) to generate *Tbc1d10c*-*CreER*^{T2};*Rosa26*^{mT/mG} bigenic mice. *Rag2*^{-/-},³⁴ *OT-I* transgenic,³⁵ and *OT-II* transgenic³⁶ mice were acquired from Jackson Laboratories. *OT-I* and *OT-II*

transgenic mice were crossed to *Tbc1d10c*^{-/-} mice to generate *OT-I*;*Tbc1d10c*^{-/-} and *OT-II*;*Tbc1d10c*^{-/-} lines. *Rag2*^{-/-} mice were crossed to *Tbc1d10c*^{-/-} mice to generate *Rag2*^{-/-};*Tbc1d10c*^{-/-} double null mice. All animal housing and experiments were conducted under an approved Institutional Animal Care and Use Committee protocol (Protocol number AC-AABC3509).

Antibodies and oligonucleotide sequences

Please see Supplemental Table S1 for a complete list of oligonucleotide primers and siRNAs and Supplemental Table S2 for all antibodies used in this study.

Tumor cell lines

Murine squamous cell carcinoma (SCC) cell lines SCC1 and LungMet2 were previously generated in our laboratory from FVB mice.³⁷ Murine B16-F10 melanoma and MC38 colon adenocarcinoma lines were purchased from ATCC. Ovalbumin-expressing B16-F10 melanoma cells (B16-OVA)³⁸ were kindly provided by Dr Charles Drake.

Delayed contact hypersensitivity assay

Contact hypersensitivity assays were performed with 2,4-Dinitro-1-fluorobenzene (DNFB) (Sigma Aldrich) as previously described³⁹ in *Tbc1d10c*^{+/+} and *Tbc1d10c*^{-/-} mice. Mice were sensitized by topical application of 0.5% DNFB as a hapten in a vehicle of acetone/olive oil (4:1 v/v) onto shaved abdominal skin. After 6 days, immune responses were elicited by topical application of 0.2% DNFB onto the ear. Ear thickness was measured on treated and untreated ears prior to and 24 hrs after DNFB with calipers. Epidermal swelling caused by infiltrating lymphocytes was rendered by the change in ear thickness before and after DNFB treatment (normalized to vehicle-treated mice; *n* = 5 mice per group).

Tamoxifen treatment

Normal or SCC-bearing *Tbc1d10c*-*CreER*^{T2};*Rosa26*^{mT/mG} bigenic mice were given daily intraperitoneal injections of 1 mg tamoxifen (Sigma Aldrich) in corn oil for four days to induce CreERT2 activity as a means to genetically mark *Tbc1d10c*-expressing cells with EGFP. 24 hrs after the final tamoxifen treatment, mice were sacrificed and cell suspensions from the spleen, lymph nodes, peritoneal cavity or SCC tumors were isolated and labeled with antibody panels for the specified immune lineages.

Orthotopic tumor assays

Tbc1d10c^{+/+} and *Tbc1d10c*^{-/-} mice received sub-cutaneous (s.c.) injections of 4 × 10⁵ SCC1 (FVB background) or 4 × 10⁵ MC38 or 5 × 10⁴ B16-F10 (C57Bl/6 background) cells. *Rag2*^{-/-};*Tbc1d10c*^{+/+} and *Rag2*^{-/-};*Tbc1d10c*^{-/-} mice on a C57Bl/6 background were administered 4 × 10⁵ MC38 or 5 × 10⁴ B16-OVA cells. All cells were administered in 200 μ l of Hanks's Balanced Salt Solution (Gibco) containing 50% Matrigel (Corning). For

immunotherapy SCC studies, *Tbc1d10c*^{+/+} and *Tbc1d10c*^{-/-} mice received intraperitoneal injections of 250 µg PD-1 or IgG2a isotype control or 100 µg CTL-A4 or IgG2b isotype control antibodies (BioXCell) as previously described⁴⁰ on days 3, 6 and 9 following tumor implantation. In all cases, tumor diameter measurements were recorded every 2 days with calipers. Tumor-bearing mice were designated by the presence of a growth in the flank skin greater than 50 mm in diameter and persistent for 24 hrs. When tumors reached the 2 cm diameter end point, tumors were harvested by surgical excision for cellular and biochemical analyses below. Average tumor size (mm²) and the percentage of tumor-free mice were compared between cohorts.

Tumor proliferation

For proliferation studies, orthotopic SCC tumor-bearing mice received a single intraperitoneal injection of 50 mg/kg 5-ethynyl-2'-deoxyuridine (EdU) (Invitrogen). After 24 hrs, orthotopic tumor single-cell suspensions were generated by enzymatic digestion as previously described.³⁷ EdU incorporation was detected using the Click-iT EdU Alexa Fluor 488 Imaging Kit as per manufacturer's instruction (Invitrogen) and quantified by flow cytometry using a BD Fortessa scanner (BD Biosciences).

Skin carcinogenesis

Cutaneous SCCs were induced in the skin of *Tbc1d10c-CreER*^{T2}; *Rosa26*^{mT/mG} mice as previously described using a 7,12-dimethylbenz[a]anthracene (Acros Organics)/12-O-tetradecanoylphorb-13-acetate (LC Laboratories) two-step chemical carcinogenesis protocol.³⁷ One week following the emergence of cSCCs, tumor-bearing mice received intraperitoneal injections of 1 mg tamoxifen as described above. 24 hours following tamoxifen administration, cSCCs were harvested for cellular analyses.

Isolation of primary T cells

Mouse splenic and lymph node single-cell suspensions were generated by mechanical dissociation as previously described.⁴¹ CD4 or CD8 T cells were purified from single-cell suspensions using EasySep T Cell Negative Isolation Kits as per manufacturer's instruction (STEMCELL Technologies). We routinely observed 90–95% purity of CD8 T cells by FACS analysis with no differences detected between *Tbc1d10c*^{+/+} and *Tbc1d10c*^{-/-} mice (Supplemental Figure S3). Henceforth, we refer to T cell subsets purified by negative isolation as *untouched*. For OVA peptide stimulation of OT-I transgenic CD8 T cells, wild-type CD8 T cells were first removed from recovered splenocyte cultures using EasySep T Cell Positive Isolation Kits as per manufacturer's instruction (STEMCELL Technologies). Primary human CD8 T cells were purified from the peripheral blood mononuclear cell fraction of whole blood (New York Blood Center) using the EasySep Human Naïve CD8 + T Cell Isolation Kit II as per manufacturer's instruction (STEMCELL Technologies).

Cell Culture

SCC1 and LungMet2 cells were cultured in complete FAD medium.⁴² MC38, B16, and B16-OVA cells were cultured in DMEM (Gibco) supplemented with 10% defined FBS (HyClone). In some cases, B16-OVA cells were incubated with 10 ng/mL murine recombinant IFN-γ (R&D Systems) for 24 hours to stimulate MHC I expression.⁴³ Murine and human T cells were cultured in RPMI 1640-GlutaMax (Gibco) supplemented with 10% heat-inactivated defined FBS (HyClone) and 55 µM 2-Mercaptoethanol (Gibco).

siRNA Gene Silencing

Primary murine or human CD8 T cells were electroporated with four pooled (SMARTpool) pre-designed siRNAs (Dharmacon) targeting murine *Epst11*, *Map3k3* or human *TBC1D10C* or non-targeting siRNA control (Scramble) using Mouse or Human T Cell Nucleofector Kits as per manufacturer's instruction (Lonza). Electroporated cells were recovered for 24 hrs in complete growth medium prior to downstream experimental use.

T-cell stimulation

For antibody stimulation, CD4 or CD8 T cells were plated in complete RPMI medium at 1.3×10^6 cells/cm² in wells coated with 1 µg/mL CD3 and soluble (5 µg/mL) CD28 antibodies for either 0, 24, 48 or 72 hrs or 15, 30 or 60 min. Unstimulated control cells were plated without CD3 or CD28 antibodies. For dose response studies, T cells were stimulated on plates coated with a range of 0–10 µg CD3 antibody. For OT-I transgenic CD8 T-cell stimulation, red blood cell-cleared C57Bl/6 splenocytes (2×10^6 cells/cm²) were coated with 10 µg/ml OVA₂₅₇₋₂₆₄ peptide (SIINFEKL) (GenScript). Co-cultures were incubated in complete RPMI medium for 0, 24, 48 or 72 hours at a cell density of 1×10^6 splenocytes and 5×10^5 OTI CD8 T cells/cm². OT-II transgenic CD4 T cells were stimulated on plates coated with a range of 0–300 nM OVA₃₂₃₋₃₃₉ peptide (ISQAVHAAHAEINEAGR) (GenScript). *Tbc1d10c*^{+/+} and *Tbc1d10c*^{-/-} OT-I transgenic CD8 T cells or OT-II transgenic CD4 T cells were loaded with CFSE as per manufacturer's instruction (BioLegend) and then stimulated with OVA.

T-cell proliferation assay

CD4 or CD8 T cells were pre-loaded with CFSE as per manufacturer's instruction (BioLegend) and then stimulated with CD3/CD28 antibodies or OVA peptides as described above for up to 72 h. T-cell proliferation as determined by quantification of the percentage of cells exhibiting CFSE dilution was detected by flow cytometry.

Trans-well migration assay

5×10^5 untouched CD8 T cells were loaded in 100 µl of RPMI 1640-GlutaMax media (Gibco) supplemented with 1% heat-

inactivated defined FBS (HyClone) into the upper insert of Boyden chambers (Corning). Murine recombinant Cxcl10 (PeproTech) was added to the lower chamber at concentrations of 0, 1, 10, or 100 ng/ml. After 3 h, migratory cells were counted in the media of the lower chamber and the transmigration index was calculated as follows: Index = (experimental cell count) ÷ (0 ng/ml Cxcl10 control cell count).

MC38 tumor killing assay

CFSE-loaded *OT-I;Tbc1d10c^{+/+}* and *OT-I;Tbc1d10c^{-/-}* CD8 T cells were activated for 24 h by OVA peptide stimulation as described above. MC38 cells were pre-incubated with 10 ng/ml murine recombinant Ifn- γ (R&D Systems) and OVA₂₅₇₋₂₆₄ peptide for 24 hrs and subsequently stained with PKH26 membrane dye as per manufacturer's protocol (Sigma Aldrich). FACS-sorted CD8 CFSE+ T cells were then plated with OVA-coated MC38 cells for 12 hrs at the following effector-to-target cell ratios: 1:2, 1:1, 2:1, and 4:1. In some cases, siRNA-transduced OT-I CD8 T cells were incubated at a 2:1 effector-to-target ratio. For each ratio, each T cell effector genotype was analyzed in triplicate. Cultures were harvested and stained with Fixable Viability Dye as per manufacturer's Protocol (Invitrogen), and MC38-specific lysis was quantified by flow cytometry. For control values, MC38 cells were either boiled for 5 minutes (Maximal lysis) or incubated without CD8 T cells (nonspecific lysis). Specific lysis was calculated as follows: Specific Lysis = [(Sample Lysis) - (nonspecific Lysis)] ÷ [(Maximal Lysis) - (nonspecific Lysis)].

Adoptive T-cell transfer

Untouched *OT-I;Tbc1d10c^{+/+}* and *OT-I;Tbc1d10c^{-/-}* CD4 and CD8 T cells were adoptively transferred by tail vein injection into *Rag2^{-/-}* mice. CD4 and CD8 T cells from the following genotypes were mixed at a 1:1 ratio: *OT-I;Tbc1d10c^{+/+}* CD4 and *OT-I;Tbc1d10c^{+/+}* CD8; *OT-I;Tbc1d10c^{+/+}* CD4 and *OT-I;Tbc1d10c^{-/-}* CD8; *OT-I;Tbc1d10c^{-/-}* CD4 and *OT-I;Tbc1d10c^{+/+}* CD8; and *OT-I;Tbc1d10c^{-/-}* CD4 and *OT-I;Tbc1d10c^{-/-}* CD8. A total of 2×10^6 T cells were injected per mouse. In some cases, *OT-I;Tbc1d10c^{+/+}* or *OT-I;Tbc1d10c^{-/-}* CD8 T cells alone were adoptively transferred into *Rag2^{-/-}* mice at 1×10^6 per mouse. Control groups included vehicle alone injected mice. Equivalent levels of *Tbc1d10c^{+/+}* and *Tbc1d10c^{-/-}* T-cell uptake were confirmed by FACS analysis of dissociated splenocytes from adoptive transfer mice.

RNA isolation, cDNA synthesis, and Quantitative PCR Analysis

Total RNA extracted from CD8 T cells was subjected to first strand cDNA synthesis as per manufacturer's instruction using the SuperScript III First-Strand Synthesis SuperMix kit (ThermoFisher). Quantitative PCR (QPCR) analyses for *Tbc1d10c*, *Map3k3*, *Epsti1* and *Gapdh* mRNA levels were performed with SYBR[®] Green Master Mix (Bio-Rad) in a Bio-Rad CFX96 system. Each sample was run in a triplicate. QPCR oligonucleotide primer sequences are listed in Supplemental Table S1.

Immunoblotting

Whole cell protein lysates were generated from CD8 and CD4 T cells in RIPA buffer (150 mM sodium chloride, 1.0% Triton X-100, 0.5% sodium deoxycholate, 0.1% SDS, 50 mM Tris, pH 8.0) containing a phosphatase and protease inhibitor cocktail (Sigma-Aldrich). In some cases, nuclear and cytosolic cell fractions were isolated from CD8 T cells using the NE-PER Nuclear and Cytoplasmic Extraction kit as per manufacturer's protocol (Thermo Scientific). Protein lysates were separated on 10% Tris-Glycine gels (ThermoFisher), transferred to nitrocellulose (Bio-Rad) and probed with primary antibodies followed by chemiluminescence detection. Protein levels were quantified by densitometric analysis using NIH-ImageJ software.

Tbc1d10c expression kinetics in cultured CD8 T cells

Untouched splenic wild-type CD8 T cells were stimulated with CD3/CD28 antibodies as described above for two days followed by expansion in complete RPMI media supplemented with 10 ng/ml recombinant Il-2 protein (R&D Systems) for three days. Cells were then stimulated again with CD3/CD28 antibodies at 2–5 million cells per well over the following time points: 0 min, 30 min, 1 h, 2 h, 4 h, 6 h, 12 h, and 24 h. Cells were harvested at each time point for total RNA or protein extraction ($n = 3$ replicates for each time point for RNA and protein). Unstimulated control cells were plated in the absence of CD3/CD28 antibodies. In some cases, untouched wild-type CD8 T cells were stimulated as described above, immediately following isolation from the spleen, followed by RNA and protein extraction.

Immunoprecipitation

CD8 T cells for immunoprecipitation were lysed in standard TritonX-100 lysis buffer with phosphatase and protease inhibitor cocktail (Sigma-Aldrich). 1 mM EDTA (Fisher Scientific) and 25 mM N-ethylmaleimide (Sigma-Aldrich) were also added to inhibit deubiquitinating enzymes. Samples were pre-cleaned using agarose-conjugated normal mouse IgG (Santa Cruz Biotechnology), and then protein supernatants were incubated with 5 μ g agarose-conjugated Bcl10 primary antibody (Santa Cruz Biotechnology) overnight on a rotator at 4°C. Bead supernatants were boiled in SDS-PAGE protein loading buffer for immunoblot analysis.

Tissue Immunofluorescence

SCC histological tissue sections (7 μ m thick) were blocked and probed with primary antibodies followed by detection with species-specific AlexaFluor conjugated secondary antibodies. DAPI counterstain was used to visualize nuclei. Immunofluorescence was captured using a Zeiss LSM 5 Exciter confocal microscope, and reconstructed images were generated using NIH ImageJ software.

Flow cytometry

Single-cell suspensions were generated from mechanically dissociated mouse spleens or enzymatically dissociated xenograft

tumors as previously described.^{30,34} Cell suspensions were labeled with directly conjugated primary antibodies (Supplementary Table S2) and analyzed using a BD LSRFortessa flow cytometer (BD Biosciences). For quantification, all flow cytometry data were analyzed using FlowJo software (BD Biosciences).

Single-Cell RNA sequencing

Live CD8 T cells from *Tbc1d10c*^{+/+} and *Tbc1d10c*^{-/-} spleens were captured on a microfluidic chip at approximately 5000 cells per sample and processed for single-cell RNA sequencing with the 10X Genomics Chromium 3' Solution platform.⁴⁴ cDNA synthesized by this method was amplified and sequenced on an Illumina NextSeq. Gene-barcode counts matrices were analyzed with the Seurat R package (version 4.0.3).⁴⁵ Cells with < 500 or > 42000 genes detected (Doublets) and > 20% mitochondrial gene mapped reads were filtered from downstream analyses. *Tbc1d10c*^{+/+} and *Tbc1d10c*^{-/-} CD8 T-cell cohort samples were merged into one Seurat object. The merged Seurat object was normalized and scaled by regressing out UMI count (10⁴) and percentage of mitochondrial and ribosomal genes. For dimensionality reduction, 2000 highly variable genes were identified based on their average expression and variance and used for clustering analysis. Dimensionality reduction was then performed using PCA, and UMAP plots were generated by the RunUMAP Seurat function with the first 9 PCs as input, determined by visualizing the drop off in PC variance explained using the ElbowPlot function in Seurat. CD8 T Cell Subtypes were classified and annotated using the ProjecTILs R package (version 2.0.0).⁴⁶ Briefly, the normalized expression matrix of the single-cell scRNA-seq data was provided as input, and non-T cells were filtered and batch corrected. The make_projection function was used to project the query data over the mouse lymphocytes reference data in UMAP space. Cell states were predicted for each cell using a nearest-neighbor algorithm with the cellstate.predict function, and predicted cell states were saved as functional cluster data slot in the Seurat object and plotted on UMAP. Differentially expressed genes within each cluster were filtered by cross-referencing with differentially expressed proteins identified by global proteomic analysis.

LC-MS/MS global proteomic analysis

Tbc1d10c^{+/+} and *Tbc1d10c*^{-/-} splenic CD8 T cells ($n = 3$ replicates per group), were subjected to Data Independent Acquisition (DIA)-based proteomic analysis⁴⁷ by the Proteomics and Macromolecular Crystallography Shared Resource Core at Columbia University. Peptides were prepared as previously described⁴⁸ and injected on Orbitrap Fusion™ Tribrid™ mass spectrometer MS/MS analysis. DIA data were analyzed with directDIA 2.0 (Deep learning augmented spectrum-centric DIA analysis) in Spectronaut Pulsar X software (Biognosys). The default settings were used for targeted analysis of DIA data in Spectronaut, and DIA files were searched against the mouse UniProt fasta database. Results obtained from Spectronaut were further analyzed using the

Spectronaut statistical package. Significantly changed protein abundance was determined by an unpaired *t*-test with a threshold for significance of $p < .05$ (permutation-based FDR correction) and 0.58 log2FC. Data sets can be accessed via the MassIVE repository (MSV000090556).

Experimental replicates and statistical analyses

All orthotopic tumor experiments in *Tbc1d10c*^{+/+} and *Tbc1d10c*^{-/-} mice were repeated at least twice. Adoptive cell transfer experiments were repeated once, and the ICI experiment was conducted once. All T cell activation, siRNA knock-down, tumor cell killing and immunoblotting experiments were repeated at least once. Results are expressed as mean \pm SD unless explicitly stated otherwise. Comparisons of two groups were analyzed by unpaired Student's *t*-test, and comparisons of more than two groups by one-way ANOVA with Bonferroni post hoc correction ($P < .05$). Finally, all mandatory laboratory health and safety procedures have been complied within the course of conducting the experimental work outlined in this study.

Results

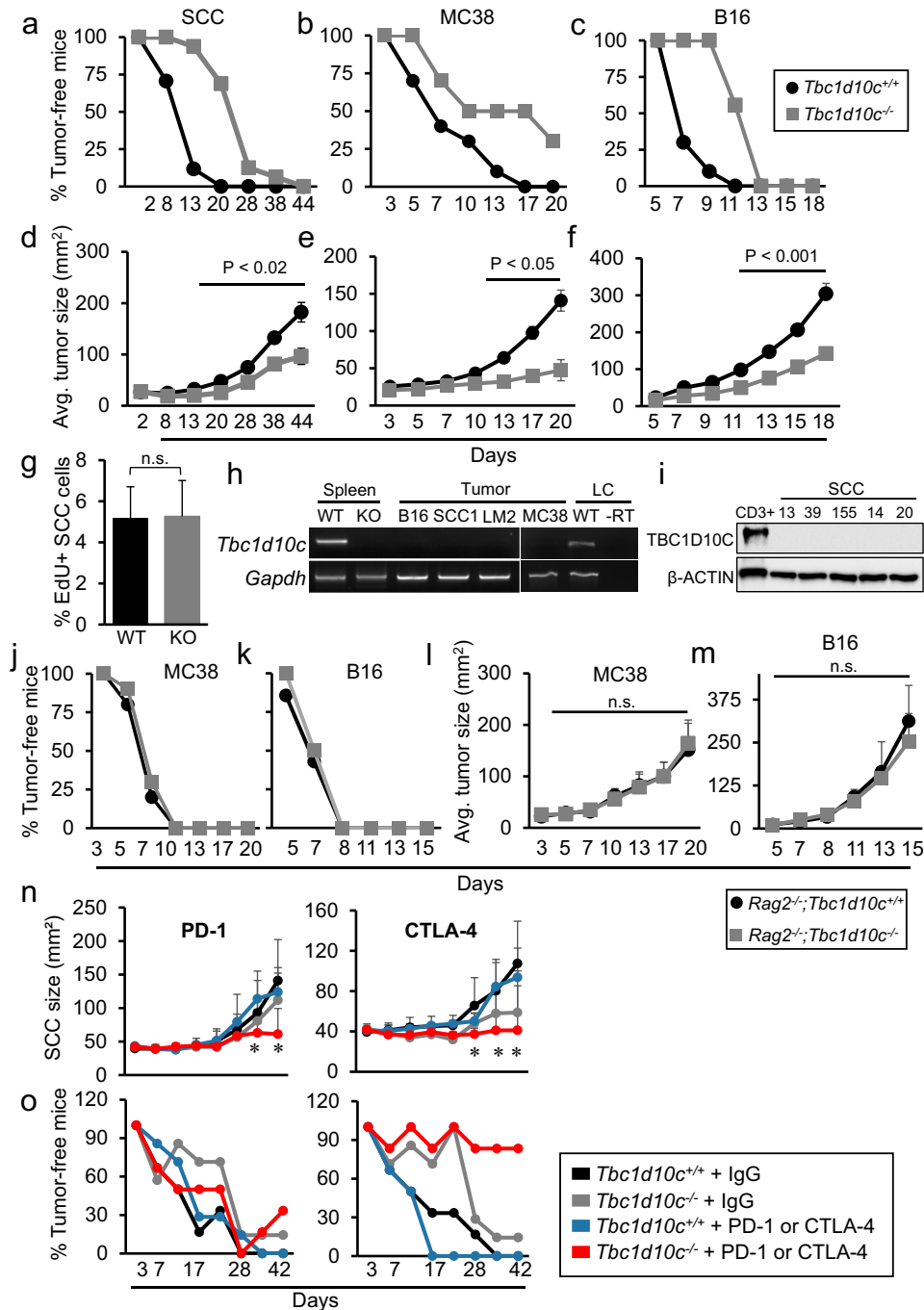
T-cell mediated tumor resistance conferred by *Tbc1d10c* deficiency

To investigate the role of *Tbc1d10c* in tumorigenesis, we generated a *Tbc1d10c* germline null (*Tbc1d10c*^{-/-}) mouse model (Supplemental Figure S1A-E). *Tbc1d10c*^{-/-} mice appear normal and show no overt phenotypic abnormalities (Supplemental Figure S1F-G) or evidence of autoimmunity in animals aged up to one year as determined by differences in skin or colon infiltrate or splenic weight (Supplemental Figure S1H-P). Given the reported roles for TBC1D10C in human and murine lymphocytes,^{25,26} we examined the steady-state levels of lymphocyte and myeloid lineages in *Tbc1d10c*^{-/-} mice. No significant changes were observed in lymphocyte composition or maturation or myeloid cell composition between *Tbc1d10c*^{+/+} and *Tbc1d10c*^{-/-} mice (Supplemental Figure S4A-I). In addition, no differences in skin contact hypersensitivity, which is commonly used as a read-out of *in vivo* CD4 T-cell activation,³⁹ were elicited in *Tbc1d10c*^{-/-} mice in response to contact allergen treatment (Supplemental Figure S4J). Collectively, these observations suggest that *Tbc1d10c* disruption does not impact immune homeostasis or dramatically perturb CD4 T-cell activation *in vivo*.

Next, we examined the sensitivity of *Tbc1d10c*^{-/-} mice to the growth of orthotopic tumors derived from weakly immunogenic B16 melanoma, highly immunogenic MC38 adenocarcinoma or a cutaneous squamous cell carcinoma (SCC) SCC1 line established in our laboratory from DMBA/TPA-treated FVB mice.³⁷ Across all three tumor types, we observed a 50–75% increase in tumor-free survival as well as a two-to-three-fold decrease in average tumor size in *Tbc1d10c*^{-/-} mice compared to *Tbc1d10c*^{+/+} mice (Figure 1A-F). To elucidate the cellular basis for the observed tumor resistance conferred by *Tbc1d10c* deficiency, we quantified tumor cell proliferation, as measured by EdU incorporation, in SCCs from *Tbc1d10c*^{+/+}

and *Tbc1d10c*^{-/-} mice. No difference in the percentages of EdU + SCC cells was observed in tumors implanted in *Tbc1d10c*^{+/+} versus *Tbc1d10c*^{-/-} mice (Figure 1G) indicating that the rate of tumor cell proliferation did not underlie the diminished growth of tumors in *Tbc1d10c*^{-/-} mice. Consistent with the

concept that *Tbc1d10c* does not directly influence tumor cell proliferation, we were unable to detect *Tbc1d10c* mRNA expression in B16 melanoma cells, two SCC cultures SCC1 and LungMet2,³⁷ or MC38 cells (Figure 1H). TBC1D10C protein was also absent in a panel of five independent human



cutaneous SCC cultures previously established in our laboratory⁴⁹ (Figure 1I). These results suggest that any pro-tumorigenic mechanism elicited by *Tbc1d10c* is likely mediated by host cells comprising the tumor microenvironment. To test this idea, we compared MC38 and B16 tumor growth in *Tbc1d10c*^{+/+} and *Tbc1d10c*^{-/-} mice crossed onto the immunocompromised *Rag2*^{-/-} background. The tumor resistance observed in immune competent *Tbc1d10c*^{-/-} mice (Figure 1B-C,E-F) was completely abolished in the absence of lymphocytes (Figure 1J-M). These data strongly suggest that tumor resistance conferred by *Tbc1d10c* deficiency is lymphocyte mediated. In addition, since *Rag2*^{-/-} mice maintain normal levels of myeloid lineages, our findings largely exclude a direct role for myeloid cells in the tumor-resistant phenotype observed *Tbc1d10c*^{-/-} mice.

To further explore the therapeutic utility of targeting *Tbc1d10c*, we performed immunotherapy checkpoint blockade experiments in SCC-bearing *Tbc1d10c*^{+/+} and *Tbc1d10c*^{-/-} mice. Treatment with either PD-1 or CTLA-4 blocking antibodies led to marked reductions in SCC size compared to IgG antibody-treated *Tbc1d10c*^{-/-} and PD-1- or CTLA-4-treated *Tbc1d10c*^{+/+} mice (Figure 1N). In addition, we observed 90% and 30% tumor-free survival in CTLA-4- and PD-1-treated *Tbc1d10c*^{-/-} mice, respectively (Figure 1O). These results suggest that combinatorial targeting of *Tbc1d10c* and immune checkpoints, particularly CTLA-4, could dramatically improve tumor outcome.

***Tbc1d10c* deficiency impacts the levels of tumor-infiltrating CD8 effectors**

To identify tumor-infiltrating *Tbc1d10c*-expressing cell lineages that may be key mediators of *Tbc1d10c* pro-tumorigenic function, we generated a *Tbc1d10c-CreER*^{T2} BAC transgenic mouse that allows for expression the tamoxifen-inducible Cre recombinase (CreERT2)⁵⁰ under the control of endogenous *Tbc1d10c* regulatory elements (Supplemental Figure S2A). For validation, *Tbc1d10c-CreER*^{T2} mice were crossed with the Cre-inducible EGFP reporter mouse, *Rosa26*^{mT/mG} to generate *Tbc1d10c-CreER*^{T2};*Rosa26*^{mT/mG} bigenic mice. We observed EGFP induction in splenic, lymph node and peritoneal cavity cells from tamoxifen-treated *Tbc1d10c-CreER*^{T2};*Rosa26*^{mT/mG} mice but not in vehicle-treated mice (Supplemental Figure S2B-D), suggesting that EGFP fluorescence is a reliable read-out for the identification of *Tbc1d10c*-expressing cells. We observed that virtually all EGFP+ cells expressed the common immune lineage marker CD45 and that EGFP marked most immune lineages, including CD3+, CD19+, CD11b+, CD11c+ and NK1.1+ in the spleen, lymph node and peritoneal cavity (Supplemental Figure S2E-H).

Next, we phenotyped tumor-infiltrating *Tbc1d10c*-expressing cells (EGFP+) in chemically induced cutaneous SCCs in *Tbc1d10c-CreER*^{T2};*Rosa26*^{mT/mG} mice. SCC-bearing mice were administered tamoxifen to induce EGFP, and tumors were analyzed by tissue immunofluorescence and FACS analyses (Figure 2A; Supplemental Figure S5A-B). In tissue sections, EGFP+ cells were abundantly detected with peri-tumoral and intra-tumoral localization (Figure 2B).

However, no EGFP was observed in Krt14+ SCC tumor keratinocytes (Figure 2B), consistent with a lack of *Tbc1d10c* expression in SCC cultures (Figure 1H-I). Flow cytometric analysis of nine independent SCCs demonstrated that tamoxifen induction of EGFP expression was restricted to CD45 + immune cells and present in a variety of immune lineages (Figure 2C). Interestingly, the vast majority (75%) of the EGFP + pool in SCCs was allocated to CD11b+ and CD8+ lineages (Figure 2C). Both CD11b+/EGFP+ and CD8+/EGFP+ cells were localized intra-tumoral (Supplemental Figure S5C-D). Next, we assessed whether there may be differences in the proportions of any tumor-infiltrating immune lineages in SCC, B16, and MC38 tumors implanted in *Tbc1d10c*^{+/+} and *Tbc1d10c*^{-/-} mice (Supplemental Figure S5A, E-I). No differences in the levels of CD4 T cells, CD4 Tregs, NK cells, CD11b +, CD11b+Gr-1+ MDSCs, CD11b+F4/80+ macrophages, CD11c+ dendritic cells or CD19 + B cells were observed between tumor cohorts (Supplemental Figure S6A-Q) (*n* = 10 tumors/group). However, two-to-three-fold increases in total CD8 T cells and two-to-nine-fold increases in Ifn-γ+ CD8 T cells were observed across SCC, B16 and MC38 tumors implanted *Tbc1d10c*^{-/-} mice (Figure 2D-I; Supplemental Figure S5H-I). Finally, the CD8/CD4 Treg ratio, a critical prognostic factor in human solid tumors, was two-fold and three-fold higher for SCC and B16 tumors, respectively, implanted in *Tbc1d10c*^{-/-} mice (Figure 2J). The observed increase in cytotoxic effectors in tumors from *Tbc1d10c*^{-/-} mice provides a cellular basis for the tumor-resistant phenotype conferred by *Tbc1d10c* deficiency.

***Tbc1d10c* suppresses CD8 T-cell activation and tumor cell killing**

To determine whether the observed increases in the levels of tumor-infiltrating Ifn-γ+ CD8 T cells in *Tbc1d10c*^{-/-} mice are due to an intrinsic role for *Tbc1d10c* in the regulation of CD8 T-cell anti-tumor function, we assessed CD8 T-cell activation and proliferation following TCR stimulation and migration in response to chemotactic cues. The *Tbc1d10c* null allele was crossed onto *OT-II* TCR transgenic (CD4 T cell analysis) or *OT-I* TCR transgenic (CD8 T cell analysis) backgrounds maintained in homogeneous C57Bl/6 strains. *OT-I*;*Tbc1d10c*^{+/+} and *OT-I*;*Tbc1d10c*^{-/-} CD8 T cells were stimulated on OVA₂₅₇₋₂₆₄ peptide-coated splenocytes followed by FACS quantification of activation markers and CFSE proliferation (Supplemental Figure S7A-B). We observed two-fold increases in the levels of CD69+, CD25+, Ifn-γ+ CD8 T cells in OVA-stimulated *OT-I*;*Tbc1d10c*^{-/-} versus *OT-I*;*Tbc1d10c*^{+/+} cohorts (Figure 3A-C). To establish human relevance for these observations in murine CD8 T cells, we silenced *TBC1D10C* expression in human CD8 T cells using siRNA pools and assessed its impact on T-cell activation. Human CD8 T cells transfected with *TBC1D10C*-targeting siRNAs exhibited an approximate 40% decrease in *TBC1D10C* protein (Supplemental Figure S8A-B) and a 1.3-fold increase in the percentage of IFN-γ + T cells following CD3/CD28 stimulation compared to CD8 T cells transfected with non-targeting control siRNA (Supplemental Figure S8C; Figure 3D). We also observed increases of 30% at 48 h and 6% at 72 h in proliferation of OVA-stimulated *OT-*

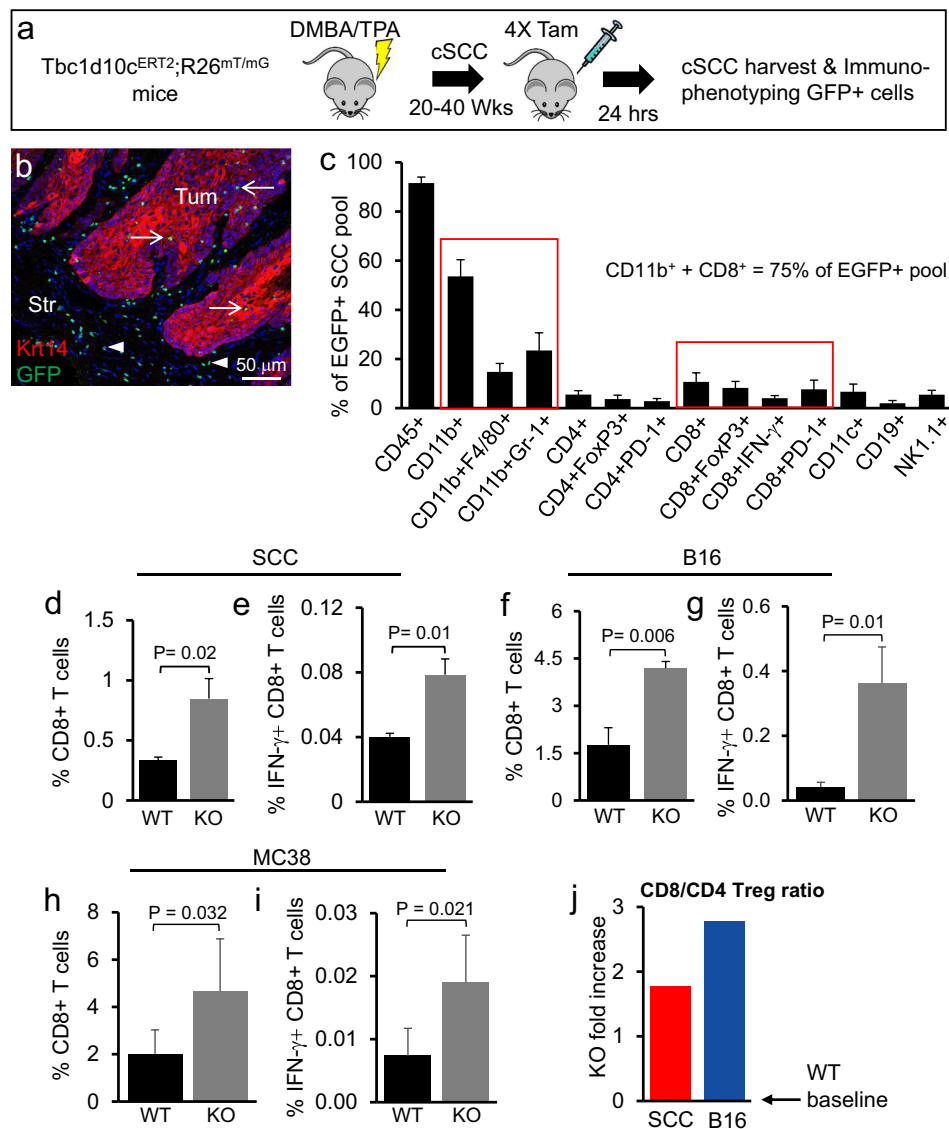


Figure 2. *Tbc1d10c* deficiency increases tumor-infiltrating CD8 effector cell levels. (A) Schematic of the experimental model for EGFP induction in chemically induced cutaneous SCCs in *Tbc1d10c-EGFP* mice. (B) Representative micrograph showing EGFP labeling and immunofluorescence detection of Krt14+ SCC tumor cells in sections of chemically induced cutaneous SCCs from tamoxifen-treated bigenic mice. (C) Bar graph showing average flow cytometric detection of *Tbc1d10c*-expressing (EGFP+) immune lineages from nine bigenic cutaneous SCCs. Red boxes group the total pool of CD11b+ or CD8+ tumor-infiltrating cells. (D-I) Bar graphs showing the average percentages of total (D,F,H) and activated (E,G,I) CD8+ T cells from SCC (D-E; $n = 4$ tumors), B16 (F-G; $n = 4$ tumors) and MC38 (H-I; $n = 6$ tumors) xenografts. P values were determined by unpaired Student's *t*-test. (J) Bar graph showing the fold-change differences in the CD8/CD4 Treg ratio for SCC and B16 tumors in *Tbc1d10c^{-/-}* mice compared to wild-type (WT ratios set at graph baseline). Abbreviations: WT, *Tbc1d10c^{+/+}*; KO, *Tbc1d10c^{-/-}*.

I; *Tbc1d10c^{-/-}* versus *OT-I*; *Tbc1d10c^{+/+}* CD8 T cells (Figure 3E; Supplemental Figure S7). However, the physiological relevance of these small, albeit significant, differences in T-cell proliferation for the tumor-resistant *Tbc1d10c^{-/-}* phenotype are likely overshadowed by the observed differences in CD8 T-cell activation. Similar levels of CD69+ or Ifn- γ + CD4 T cells or CFSE proliferation were observed between OVA-stimulated *OT-II*; *Tbc1d10c^{+/+}* and *OT-II*; *Tbc1d10c^{-/-}* cohorts (Supplemental Figure S9A-D). We did observe a two-fold increase in Il-2 + CD4 T cells in the *OT-II*; *Tbc1d10c^{-/-}* cohort at 72 h of OVA stimulation; however, this difference occurred during the decline of Il-2+ cell levels compared to peak activation at the 24-h time point (Supplemental Figure S9B). For CD3/CD28 stimulation, we observed similar percentages of Il-2 + CD4 T cells and CFSE proliferation between *Tbc1d10c^{+/+}*

and *Tbc1d10c^{-/-}* cohorts (Supplemental Figure S9E-F). The similar levels of CD4 T-cell activation between OVA- and CD3/CD28-stimulated *Tbc1d10c^{+/+}* and *Tbc1d10c^{-/-}* CD4 T-cell cohorts are consistent with the similar responses between *Tbc1d10c^{+/+}* and *Tbc1d10c^{-/-}* mice to contact allergens *in vivo* (Supplemental Figure S4J). Finally, we employed a well-established trans-well migration assay to measure CD8 T-cell migration in response to increased concentration gradients of the chemokine Cxcl10.⁵¹ We observed similar levels (approximately 25%) of untouched CD8 T cells expressing the Cxcl10 receptor, Cxcr3 (Supplemental Figure S9G-H) and a Cxcl10 dose-dependent increase in the numbers of migrating *Tbc1d10c^{+/+}* and *Tbc1d10c^{-/-}* CD8 T cells (Figure 3F). However, no increased migration was observed in *Tbc1d10c^{-/-}* CD8 T cells (Figure 3F). Collectively, our findings indicate

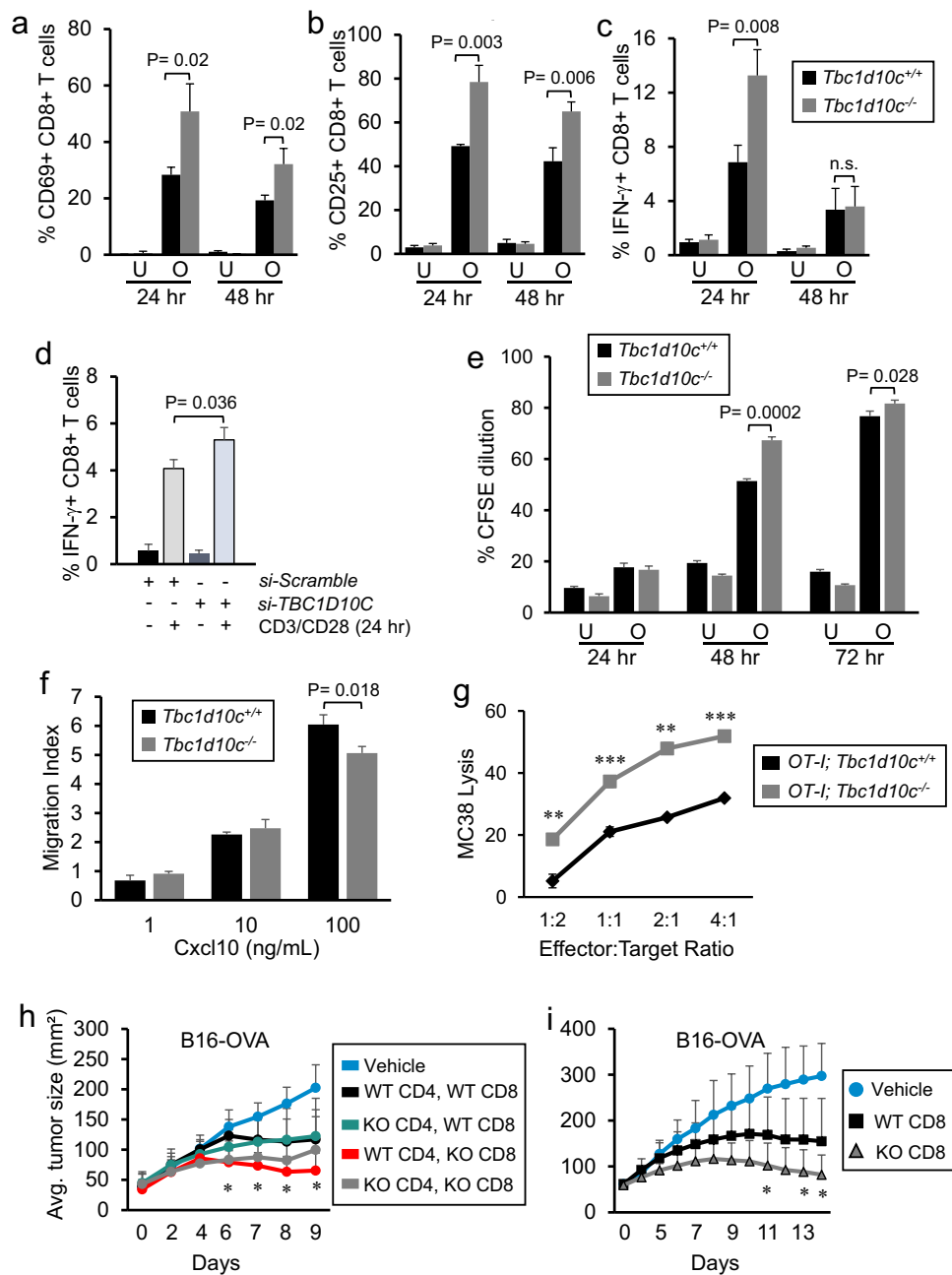


Figure 3. *Tbc1d10c* is an intrinsic suppressor of CD8 T-cell activation and cytotoxic function. (A-C) Bar graphs showing the average percentages of CD69+ (A), CD25+ (B) and IFN- γ + (C) CD8 T cells from OT-I;*Tbc1d10c*^{+/+} and OT-I;*Tbc1d10c*^{-/-} mice either unstimulated (U) or stimulated (O) with OVA peptide for the indicated times ($n = 3$ replicates per group). (D) Bar graphs showing flow cytometric detection of IFN- γ + primary human CD8 T cells transfected with non-targeting (Scramble) or TBC1D10C-targeting siRNA pools ($n = 3$ replicates per group). (E) Bar graphs showing proliferation as measured by CFSE dilution in CD8 T cells from OT-I;*Tbc1d10c*^{+/+} and OT-I;*Tbc1d10c*^{-/-} mice either unstimulated (U) or stimulated (O) with OVA peptide for the indicated times ($n = 3$ replicates per group). (F) Bar graphs showing the average migration index of CD8 T cells from *Tbc1d10c*^{+/+} and *Tbc1d10c*^{-/-} mice in the presence of 1, 10, and 100 ng/ml Cxcl10 ($n = 3$ replicates per group). (G) Line graphs showing average MC38 cell lysis by OT-I;*Tbc1d10c*^{+/+} and OT-I;*Tbc1d10c*^{-/-} CD8 T cells ($n = 3$ replicates per ratio group). (H-I) Line graph showing average B16-OVA tumor size in *Rag2*^{-/-} mice adoptively transferred with OT-I CD4 and CD8 T cells (H; $n = 5$ mice per group) or OT-I CD8 T cells alone (I; $n = 9$ mice per group) carrying the indicated (WT or KO) *Tbc1d10c* genotype. P values were determined by unpaired Student's *t*-test. Abbreviation: n.s., not significant.

that *Tbc1d10c* deficiency primarily impacts CD8 T-cell activation, and not proliferation or migration, following TCR ligation.

To assess the relevance of enhanced CD8 T-cell activation conferred by *Tbc1d10c* deficiency for cytotoxic effector function, we assessed the tumor cell killing capacity of OT-I;*Tbc1d10c*^{+/+} and OT-I;*Tbc1d10c*^{-/-} CD8 T cells against OVA peptide-bearing MC38 tumor cells. We observed an

effector cell dose response increase in tumor cell lysis for both OT-I;*Tbc1d10c*^{-/-} and OT-I;*Tbc1d10c*^{+/+} CD8 T cell cohorts (Supplemental Figure S10; Figure 3G). MC38 cell lysis was increased two- to three-fold across all effector-to-target ratios in OT-I;*Tbc1d10c*^{-/-} compared to OT-I;*Tbc1d10c*^{+/+} CD8 T cells (Figure 3G). These results suggest that the augmented CD8 T-cell activation and effector function in *Tbc1d10c*^{-/-} mice are sufficient to confer the tumor-resistant

phenotype. To test this idea, we performed adoptive cellular transfer of CD4 and CD8 T cells into B16-OVA-bearing *Rag2*^{-/-}; *Tbc1d10c*^{+/+} mice. Mice received adoptive transfer combinations of CD4 and CD8 T cells from *OT-1*; *Tbc1d10c*^{+/+} or *OT-1*; *Tbc1d10c*^{-/-} mice. In some cases, *OT-1* CD4 and CD8 T-cell combinations were mixed from *Tbc1d10c*^{+/+} and *Tbc1d10c*^{-/-} genotypes. B16-OVA-bearing *Rag2*^{-/-}; *Tbc1d10c*^{+/+} mice adoptively transferred with *Tbc1d10c*^{-/-} CD8 T cells, regardless of the CD4 T-cell *Tbc1d10c* genotype, exhibited the most resistance to tumor growth (Figure 3H). In a separate set of experiments, B16-OVA-bearing *Rag2*^{-/-}; *Tbc1d10c*^{+/+} mice were adoptively transferred with *OT-1*; *Tbc1d10c*^{+/+} or *OT-1*; *Tbc1d10c*^{-/-} CD8 T cells alone. A two-fold reduction in melanoma size was observed in mice transferred with *OT-1*; *Tbc1d10c*^{-/-} compared with *OT-1*; *Tbc1d10c*^{+/+} CD8 T cells (Figure 3I), which fully recapitulates the tumor-resistant phenotype observed in immune competent *Tbc1d10c*^{-/-} mice (Figure 1). Collectively, these observations confirm that tumor resistance conferred by *Tbc1d10c* deficiency is mediated by CD8 T cells.

RNA and proteomic profiling of *Tbc1d10c*^{-/-} CD8 T cells

To identify signaling pathways that may be impacted by *Tbc1d10c* disruption that are also relevant for CD8 T-cell-mediated anti-tumor immunity, we conducted single-cell RNA sequencing (scRNA-Seq) of untouched *Tbc1d10c*^{+/+} and *Tbc1d10c*^{-/-} CD8 T cells. Unsupervised clustering of *Tbc1d10c*^{+/+} and *Tbc1d10c*^{-/-} cohorts identified similar distributions of CD8 T-cell clusters and that *Tbc1d10c* was ubiquitously expressed across all CD8 T-cell subsets (Supplemental Figure S11A-B) suggesting that *Tbc1d10c* loss does not lead to a spontaneous CD8 T-cell phenotype. To investigate the impact of *Tbc1d10c* deficiency on functionally relevant CD8 T cell subsets, we utilized ProjecTILs and its mouse lymphocyte reference atlas to interpret CD8 T-cell states⁴⁶ between *Tbc1d10c*^{+/+} and *Tbc1d10c*^{-/-} cohorts. ProjecTILs classified most CD8 T cells as Naïve cells in both genotypes, and no significant changes in memory and early active subsets between *Tbc1d10c*^{+/+} and *Tbc1d10c*^{-/-} cohorts were observed (Figure 4A-B). scRNA-Seq also demonstrated that *Tbc1d10c* was ubiquitously expressed across all CD8 T-cell subsets in both genotypes (Figure 4C).

Since no perturbations in specific CD8 T-cell subsets were observed in unsupervised clustering (Supplemental Figure S11A) and *Tbc1d10c* was broadly expressed in all CD8 T cells (Figure 4C); Supplemental Figure S11B), we opted for a computational strategy that would integrate *Tbc1d10c*^{+/+} and *Tbc1d10c*^{-/-} CD8 T-cell data sets to identify differentially expressed genes (DEGs) that were common across all or most CD8 T-cell clusters. Integrated analysis identified 3023 DEGs across 15 clusters ($P_{\text{Adj}} < 0.05$; Top 25 DEGs shown in Figure 4D). To help prioritize the list of 3023 scRNA-Seq DEGs, we performed global proteomics profiling of *Tbc1d10c*^{+/+} and *Tbc1d10c*^{-/-} CD8 T cells, which identified a total of 331 differentially expressed candidates in *Tbc1d10c*^{-/-} CD8 T cells ($P_{\text{Adj}} < 0.05$; Supplemental Table S3). Next, we employed immunoblot analysis of *Tbc1d10c*^{+/+} and *Tbc1d10c*^{-/-} CD8 T-cell lysates and observed that the

following categories of DEGs failed validation by immunoblot analysis: DEGs identified only by scRNA-Seq, such as *Hspa8*, *Syk* and *Cxcr4*, DEGs identified only by global proteomics, such as *Stat3*, or DEGs identified by both profiling approaches but were unique to an individual cluster by scRNA-Seq analysis, such as *Runx3* (Supplemental Figure S11C-D). Since *Stat3* was identified by proteomics to be enriched approximately two-fold in *Tbc1d10c*^{-/-} CD8 T cells (Supplemental Table S3), we analyzed *Tbc1d10c*^{-/-} CD8 T-cell lysates for *Stat1*, *Stat3* and *Stat5* expression levels given the well-established role for the JAK-STAT pathway in T-cell activation. However, highly analogous protein levels for all Stat proteins were observed between CD8 T-cell cohorts (Supplemental Figure S11E).

Given the broad expression of *Tbc1d10c* across CD8 T cells (Figure 4C; Supplemental Figure S11B), we posited that DEGs specific to an individual CD8 T-cell cluster may not be validated at the protein expression level, thereby diminishing the relevance as a key mediator of *Tbc1d10c* signaling. As such, to facilitate the identification of critical DEGs in *Tbc1d10c*^{-/-} CD8 T cells, we cross-referenced DEG lists from the integrated scRNA-Seq and global proteomics analyses and identified nine candidates that were common to both profiling assays. Of these nine candidates, only two, *Dnaj1* and *Epsti1*, were significantly different across all scRNA-Seq CD8 T-cell clusters (Figure 4D-E). While *Epsti1* was consistently downregulated at mRNA and protein levels in *Tbc1d10c*^{-/-} CD8 T cells, *Dnaj1* protein and mRNA differences were inconsistent (Figure 4D-E). Immunoblot analysis confirmed a 50% decrease in *Epsti1* protein levels in *Tbc1d10c*^{-/-} compared to *Tbc1d10c*^{+/+} CD8 T cells, but no difference in *Dnaj1* protein levels (Figure 4F). As such, we focused on a potential role for *Epsti1* as an effector of *Tbc1d10c* signaling in CD8 T cells.

QPCR analysis confirmed a 50% reduction in *Epsti1* mRNA expression in *Tbc1d10c*^{-/-} CD8 T cells (Figure 4G). *Epsti1* protein downregulation was maintained following CD3/CD28 TCR stimulation for 24 h (Figure 4H-I), suggesting that the perturbed expression of *Epsti1* may also be relevant for the observed augmented activation of *Tbc1d10c*^{-/-} CD8 T cells. *Epsti1* regulates the 26S proteasomal degradation of $\text{I}\kappa\text{B}\alpha$,⁵² which is a key suppressor of p65 transactivation in the NF- κB pathway.⁵³ Therefore, we also assessed $\text{I}\kappa\text{B}\alpha$ mRNA and protein levels in *Tbc1d10c*^{+/+} and *Tbc1d10c*^{-/-} CD8 T cells. While no difference in $\text{I}\kappa\text{B}\alpha$ mRNA expression was observed in *Tbc1d10c*^{-/-} CD8 T cells (Figure 4G), we identified a 40% decrease in total $\text{I}\kappa\text{B}\alpha$ protein in unstimulated and TCR-stimulated *Tbc1d10c*^{-/-} CD8 T cells (Figure 4H-I). The observed downregulation of $\text{I}\kappa\text{B}\alpha$ protein in *Tbc1d10c*^{-/-} CD8 T cells is inconsistent with the established role for *Epsti1* in promoting $\text{I}\kappa\text{B}\alpha$ protein degradation in B cells.⁵² This observation suggests that either *Epsti1* does not regulate $\text{I}\kappa\text{B}\alpha$ protein levels in CD8 T cells or that additional mechanisms are involved in $\text{I}\kappa\text{B}\alpha$ protein homeostasis in the context of *Tbc1d10c* disruption. To address these issues and whether *Epsti1* downregulation is responsible for the CD8 T-cell activation phenotype due to *Tbc1d10c* deficiency, we assessed the impact of silencing *Epsti1* mRNA in *Tbc1d10c*^{+/+} CD8 T cells on $\text{I}\kappa\text{B}\alpha$ protein levels and T-cell activation. *Epsti1* siRNA-transfected cells exhibited a 50% reduction in protein

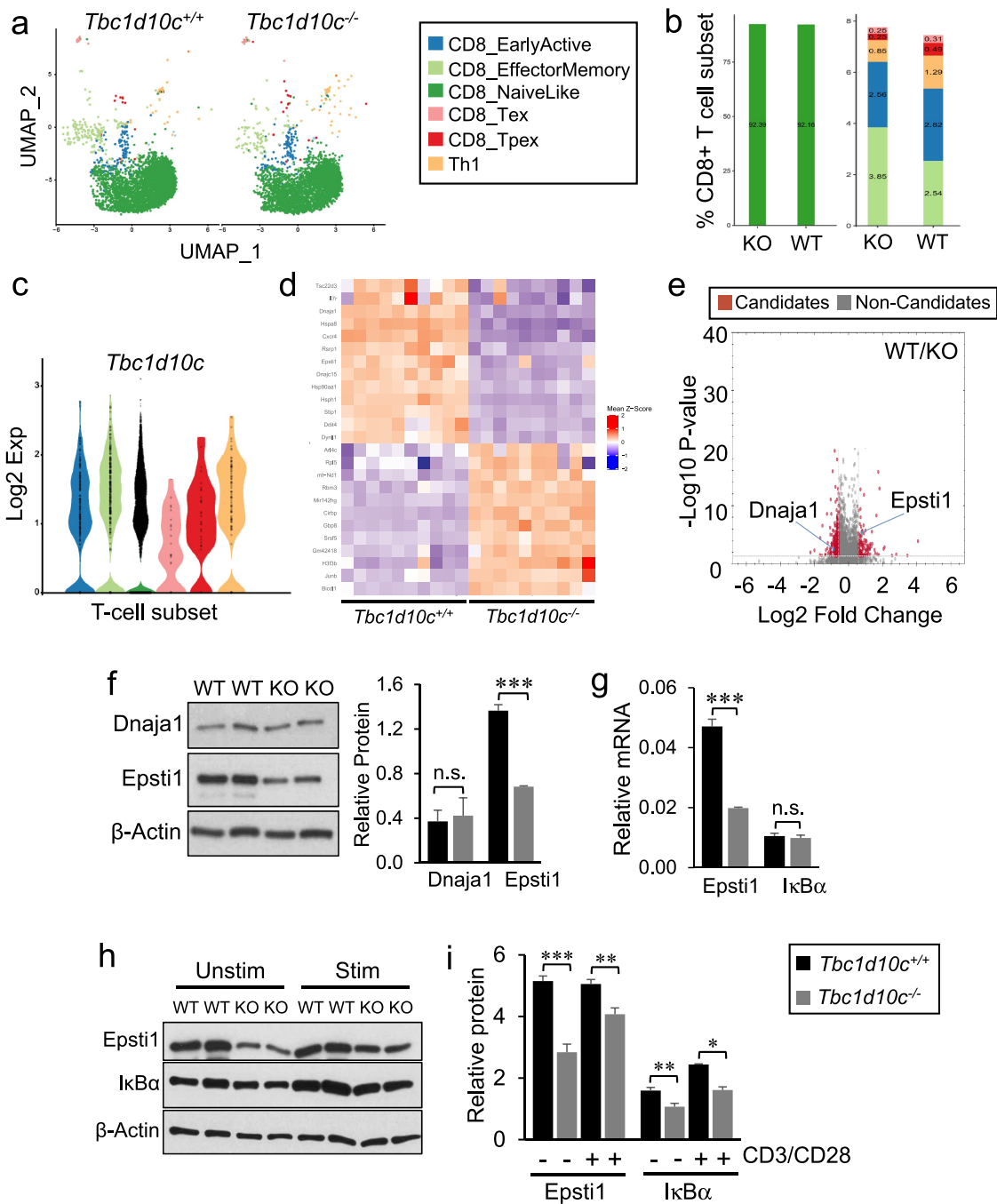


Figure 4. Single-cell RNA sequencing and dual LC-MS/MS proteomic profiling in *Tbc1d10c*^{-/-} CD8 T cells. (A) Two-dimensional uniform manifold approximation and projection (UMAP) visualization of CD8 T-cell subsets generated by ProjectTILs analysis (cells were projected to the mouse reference TIL atlas) of scRNA-seq *Tbc1d10c*^{+/+} and *Tbc1d10c*^{-/-} data sets. Each point represents a single cell and T-cell subsets are color-coded (middle box). (B) Bar plots comparing the quantified percentages of naïve-like (left) and memory, early active and Th1 (right) CD8 T-cell subsets, according to the ProjectTILs analysis, between *Tbc1d10c*^{+/+} and *Tbc1d10c*^{-/-} cohorts. (C) Violin plot showing mRNA expression of *Tbc1d10c* across CD8 T-cell subsets. Each black dot represents a cell, and T-cell subtypes are color-coded. (D) Mean-z score heatmap showing the arithmetic mean of the z scores for the top 25 DEGs CD8⁺ T cells in *Tbc1d10c*^{+/+} and *Tbc1d10c*^{-/-} scRNA-Seq integrated data sets ($P_{Adj} < 0.05$). (E) Volcano plot from LC-MS/MS global proteomic analysis of *Tbc1d10c*^{+/+} and *Tbc1d10c*^{-/-} CD8 T cells ($n = 3$ replicates per group, P values determined by unpaired Student's *t*-test with permutation-based FDR correction). (F) Gel images and bar graph (densitometric quantification) showing immunoblot detection of Dnaja1 and Epsti1 in *Tbc1d10c*^{+/+} and *Tbc1d10c*^{-/-} CD8 T-cell lysates ($n = 2$ replicates per group). (G) Bar graphs showing relative mRNA expression of Epsti1 and IκBα as determined by qPCR ($n = 3$ per replicates per group). (H-I) Gel images (H) and densitometric quantification (I) of relative Epsti1 and IκBα protein levels in unstimulated and CD3/CD28-stimulated cells ($n = 2$ replicates per group). P values were determined by unpaired Student's *t*-test (*, < 0.05 ; **, < 0.04 ; ***, < 0.02).

expression compared to si-Scramble-transfected cells (Figure 5A-B), which closely resembles Epsti1 downregulation in *Tbc1d10c*^{-/-} CD8 T cells (Figure 4). As reported in B cells,⁵² Epsti1 knockdown in wild-type CD8 T cells led to a two-fold increase in IκBα protein levels in CD3/CD28 TCR-stimulated cells (Figure 5A-B). However, Epsti1-knockdown cells actually

exhibited reduced levels of activation markers, including CD69, Ifn-γ and Tnf-α, following TCR stimulation (Supplemental Figure S12A; Figure 5C). These observations indicate that IκBα protein downregulation and augmented activation levels observed in *Tbc1d10c*^{-/-} CD8 T cells are likely not due to Epsti1 downregulation. As such, Epsti1 is not the

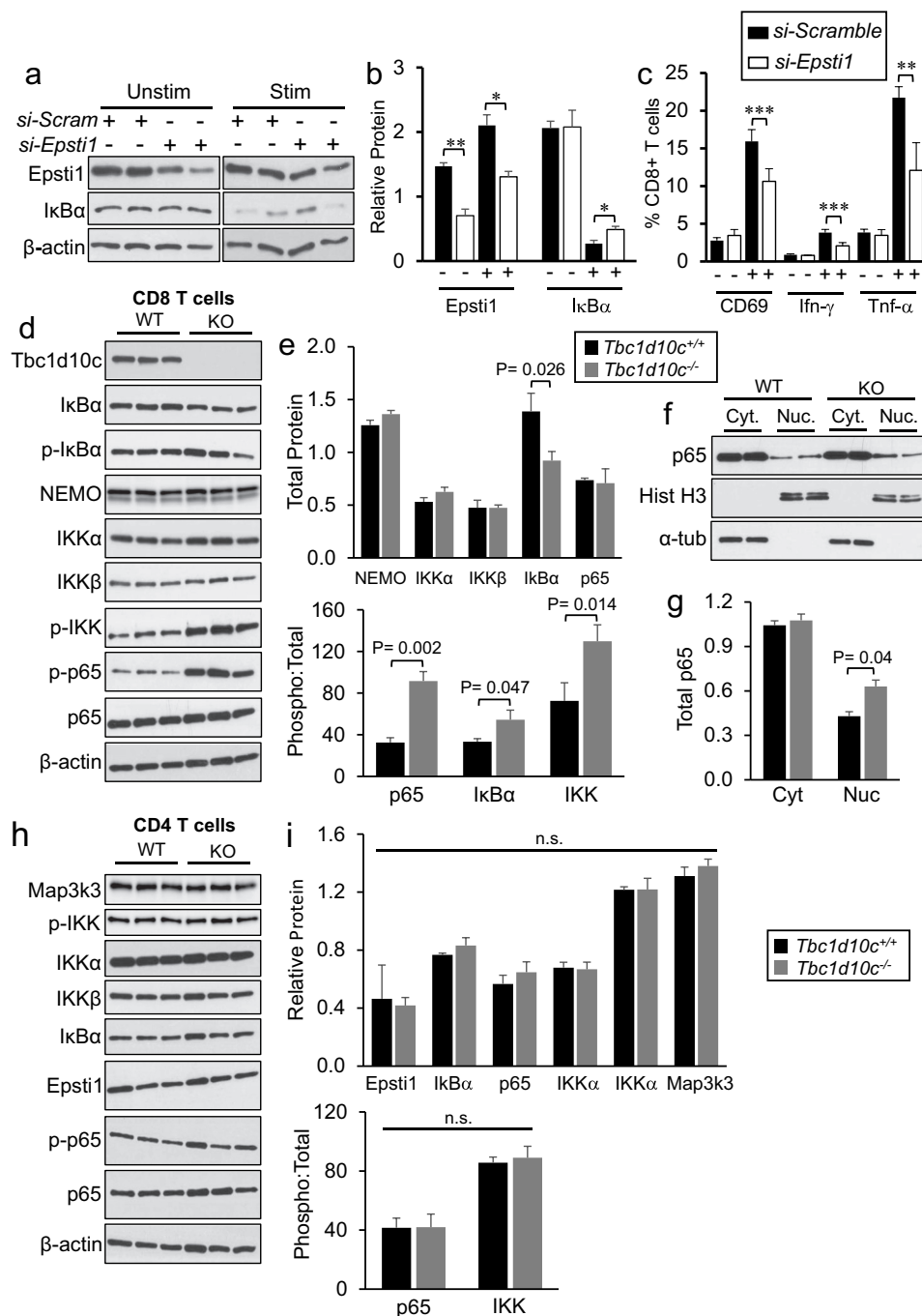


Figure 5. NF-κB pathway activation in CD8 T cells. (A-B) Gel images (A) and densitometric quantification bar graphs (B) showing relative protein levels for Epsti1 and IκBα in wild-type CD8 T cells after siRNA knockdown of *Epsti1* ($n = 2$ replicates per group). (C) Bar graphs showing the average percentages of si-Scramble- or si-*Epsti1*-transduced CD8 T cells positive for CD69 (A), Ifn-γ (B) or Tnf-α (C) following 24 hr co-stimulation with CD3/CD38 antibodies. (D-I) Gel images and densitometric quantification (bar graphs) showing relative protein levels for CD8 T-cell lysates (D-G) or CD4 T-cell lysates (H-I) of total and phosphorylated protein levels of canonical NF-κB pathway members ($n = 3$ per replicates per group). Abbreviations: Cyt, cytoplasmic fraction; Nuc, nuclear fraction. P values were determined by unpaired Student's *t*-test.

primary effector responsible for the *Tbc1d10c* null phenotype. However, IκBα is a known inhibitor of NF-κB pathway activity,⁵³ which is a crucial component of TCR activation.⁵⁴ Our data suggest that *Tbc1d10c* signaling mediates post-translational regulation of IκBα and thus may suppress downstream NF-κB activity.

To test this assertion, we quantified the total and activated (phosphorylated) levels of members of the canonical NF-κB pathway downstream of IκBα in *Tbc1d10c*^{+/+} and *Tbc1d10c*^{-/-}

CD8 T cells by immunoblot analysis. As expected, we observed a 50% decrease in total IκBα protein in *Tbc1d10c*^{-/-} CD8 T cells; however, no differences in the total levels of IKK complex members, IKKα, IKKβ or Nemo, or p65 were detected (Figure 5D-E). Strikingly, the phosphorylated levels of IκBα, IKK and p65 were dramatically higher in *Tbc1d10c*^{-/-} CD8 T cells (Figure 5D-E) culminating in two-to-three-fold increases in the ratio of phosphorylated-to-total protein for these downstream NF-κB pathway members (Figure 5E).

Next, we analyzed the nuclear and cytosolic fractions of *Tbc1d10c*^{+/+} and *Tbc1d10c*^{-/-} CD8 T cells to determine whether the observed increase in p65 phosphorylation (Figure 5D-E) correlated with increased nuclear localization. Nuclear p65 levels were approximately two-fold higher in untouched *Tbc1d10c*^{-/-} CD8 T cells without a discernible change in cytosolic p65 levels (Figure 5F-G). The canonical NF- κ B pathway downstream of TCR activation is generally thought to be analogous between CD4 and CD8 T cells; however, our *Tbc1d10c*^{-/-} T-cell activation phenotype is highly skewed toward CD8 T cells. Therefore, we also analyzed the total and phosphorylated protein levels of NF- κ B pathway members in CD4 T cells. Interestingly, we observed no quantifiable differences in total or phosphorylated forms of Epst1 or any NF- κ B pathway proteins in *Tbc1d10c*^{-/-} CD4 T cells (Figure 5H-I). Finally, a significant, but modest increase (25%) in Tbc1d10c protein levels was observed in CD4 compared to CD8 T cells (Supplemental Figure S12B). These observations further strengthen the mechanistic relevance for Tbc1d10c suppression of NF- κ B pathway activity specifically in CD8 T-cell activation.

Our findings above correlate downregulation of the NF- κ B pathway inhibitor I κ B α with increased activation of canonical NF- κ B pathway proteins including IKK α / β and p65. To determine whether these observations in untouched CD8 T cells hold functional relevance for the increased activation levels in *Tbc1d10c*^{-/-} CD8 T cells following TCR stimulation, we assessed total and phosphorylated IKK and p65 levels during a time course of CD3/CD28 TCR stimulation. While no differences in total protein levels were observed, the average percentages of phosphorylated p65 and IKK β were significantly higher in *Tbc1d10c*^{-/-} compared to *Tbc1d10c*^{+/+} CD8 T cells at 15, 30 and 60 min after CD3/CD28 TCR stimulation (Figure 6A-B). Importantly, these observations provide a mechanistic link between perturbed NF- κ B pathway activation and the augmented response of *Tbc1d10c*^{-/-} CD8 T cells to TCR stimulation. To bridge our observations of upregulated NF- κ B pathway activation and CD8 T-cell activation following TCR stimulation to the increased levels of activated tumor-infiltrating CD8 T cells and tumor resistance phenotype in *Tbc1d10c*^{-/-} mice, we quantified the activated (phosphorylated) levels of IKK proteins in tumor-infiltrating CD8 T cells from SCCs implanted in *Tbc1d10c*^{+/+} and *Tbc1d10c*^{-/-} mice by Phosflow analysis. We observed a 2.5-fold increase in p-IKK+ CD8 T cells in SCCs from *Tbc1d10c*^{-/-} mice (Figure 6C-D), indicating that augmented NF- κ B signaling observed in *Tbc1d10c*^{-/-} CD8 T cells from healthy spleen is mechanistically relevant for the augmented anti-tumor response in tumor-infiltrating *Tbc1d10c*^{-/-} CD8 T cells. Importantly, p-IKK levels were also significantly increased in primary human CD8 T cells transfected with si-*TBC1D10C* compared to non-targeting transfected cells in both unstimulated and CD3/CD28 TCR-stimulated cohorts (Figure 6E-F).

In both murine and human CD8 T cells, Tbc1d10c deficiency leads to increased activation levels of canonical NF- κ B pathway members even in untouched murine and unstimulated human cells. These observations primarily implicate Tbc1d10c as a constitutive suppressor of the NF- κ B pathway in CD8 T cells. Tbc1d10c was previously classified as a feedback inhibitor of TCR

activation in human CD4 T cells based on its low expression in unstimulated and rapid induction in TCR-stimulated CD4 T cells and its ability to bind and inhibit Calcineurin and Ras signaling.²⁵ In both murine and human CD8 T cells, we observed robust *Tbc1d10c* mRNA and protein expression in untouched or unstimulated cells and up to eight-fold downregulation of *Tbc1d10c* mRNA and three-fold downregulation of protein following TCR stimulation (Supplemental Figure S13). We also observed similar levels of nuclear NFAT1, as a read-out of Calcineurin signaling activity, and phosphorylated ERK1/2 following TCR ligation in *Tbc1d10c*^{+/+} and *Tbc1d10c*^{-/-} CD8 T cells (Supplemental Figure S14).

***Tbc1d10c* deficiency perturbs NF- κ B signaling via Map3k3 stability**

Our findings above illustrate a mechanistic role for Tbc1d10c in suppressing NF- κ B pathway activation following TCR ligation in CD8 T cells. To further explore the mechanism by which Tbc1d10c signaling suppresses NF- κ B pathway activation, we analyzed the status of TCR signaling proteins known to be upstream of IKB phosphorylation. First, we performed CD3/CD28 TCR stimulation experiments with CD3 alone, CD28 alone, or CD3/CD28 co-stimulation in order to determine whether Tbc1d10c may intersect one of these pathways individually upstream of the merge with PKC- θ .⁵⁵ CD3/CD28 co-stimulation led to the expected increases in *Tbc1d10c*^{-/-} CD8 T-cell activation markers CD69, Ifn- γ , and Tnf- α (Supplemental Figure S15A-D), corroborating our findings with OVA peptide stimulation of OT-I CD8 T cells (Figure 3). However, there were no differences in the residual levels of these activation markers in CD8 T cells in the presence of CD3 or CD28 alone (Supplemental Figure S15A-D) indicating that Tbc1d10c does not directly impact either of these pathways upstream of PKC- θ . No difference in total or phosphorylated levels of PKC- θ was observed between *Tbc1d10c*^{+/+} and *Tbc1d10c*^{-/-} CD8 T cells (Figure 6G-H). The CARMA1-Bcl10-MALT1 (CBM) signalosome complex is directly downstream of PKC- θ and serves to recruit and activate the IKK complex upon TCR ligation.⁵⁶ Within the CBM, Bcl10 upregulation is sufficient for downstream NF- κ B transactivation.⁵⁷ We observed a modest (20%) increase in total Bcl10 protein levels (Figure 6G,I), which was likely due to a 40% upregulation of Bcl10 mRNA expression (Figure 6J) in *Tbc1d10c*^{-/-} CD8 T cells. No perturbations were observed in Bcl10 protein ubiquitination (Supplemental Figure S15E-F), suggesting that the increased Bcl10 mRNA and protein expression likely resulted from a p65-mediated positive feedback loop on Bcl10 regulation^{58,59} rather than changes in protein stabilization. No differences in total TAK1 or phosphorylated TAK1 protein levels were observed in *Tbc1d10c*^{-/-} CD8 T cells (Figure 6G, K), which largely excludes a direct role for TAK1 in the observed two-to-three-fold increases in p-IKK levels (Figure 5). Collectively, these findings indicate that increased activation of the IKK complex is the furthest upstream target in the canonical NF- κ B pathway impacted by Tbc1d10c deficiency. As such, our results suggest that Tbc1d10c likely intersects canonical NF- κ B signaling via a mediator of IKK complex phosphorylation from a heterologous pathway.

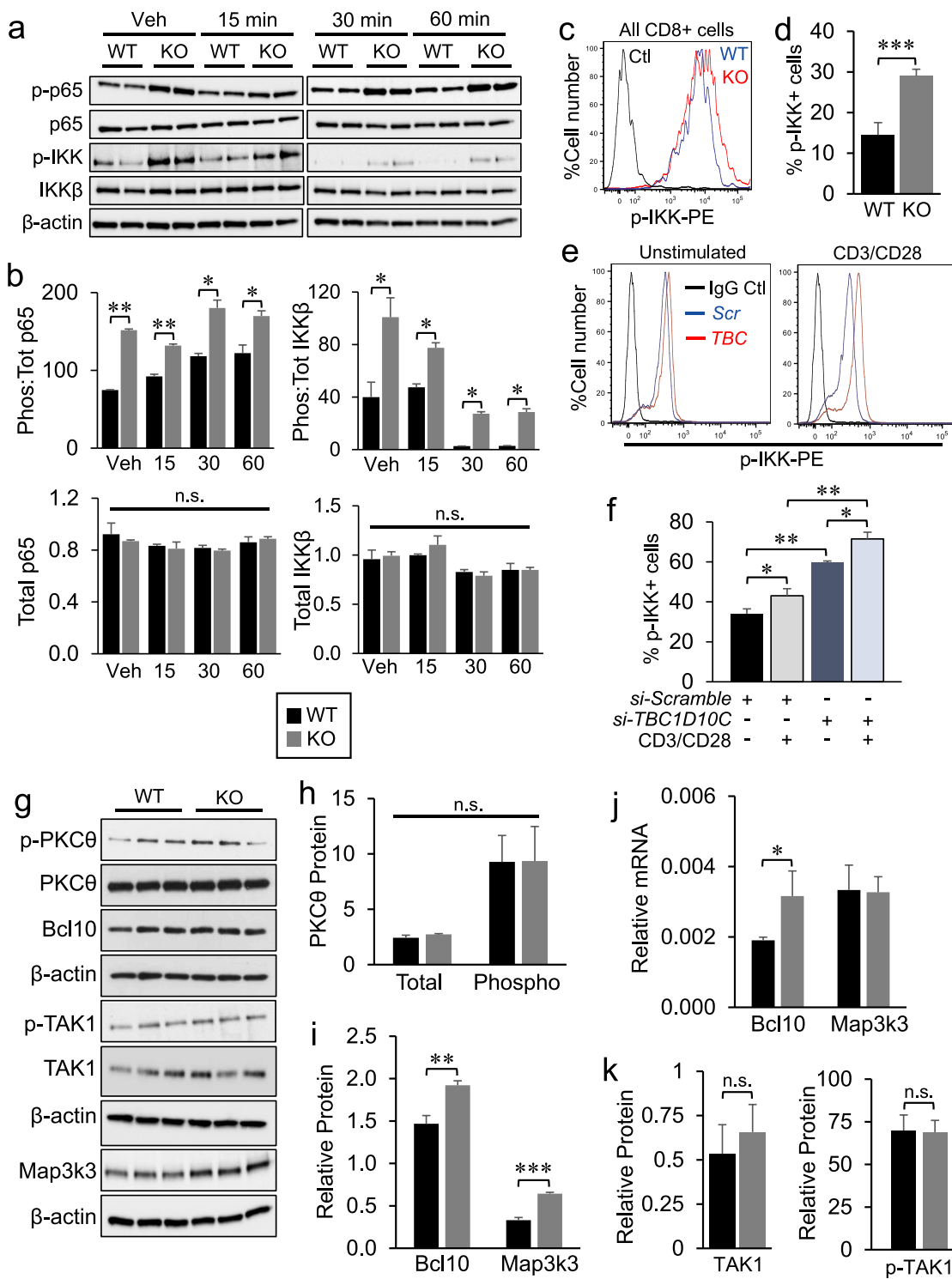


Figure 6. Assessment of I κ B α and Map3k3 expression in *Tbc1d10c*^{-/-} CD8 T cells. (A-B) Gel images (A) and densitometric quantification (B) of total and phosphorylated p65 and IKK β protein levels in *Tbc1d10c*^{+/+} and *Tbc1d10c*^{-/-} CD8 T cells following CD3/CD28 activation at the indicated time points ($n = 2$ replicates per group). (C-D) Representative dot plots of flow cytometric detection of p-IKK levels of SCC-infiltrating CD3+ CD8 + T cells and bar graph (D) showing average percentage of p-IKK+ CD8 T cells ($n = 4$ tumors per group). Histogram shows an overlay of representative p-IKK+ cell numbers in *Tbc1d10c*^{+/+} and *Tbc1d10c*^{-/-} cohorts. (E) Representative dot plots of flow cytometric detection of p-IKK+ human CD8 T cells subjected to TBC1D10C siRNA or control (si-Scramble) silencing and vehicle (unstimulated) or CD3/CD28 stimulation. (F) Bar graph showing the average percentage of p-IKK+ human CD8 T cells subjected to TBC1D10C siRNA or control (si-Scramble) silencing and CD3/CD28 stimulation ($n = 5$ replicates per group). (G-I) Gel images and densitometric quantification (bar graphs) showing relative total and phosphorylated protein levels of indicated proteins in *Tbc1d10c*^{+/+} and *Tbc1d10c*^{-/-} CD8 T cells ($n = 3$ replicates per group). (J) Bar graphs showing relative mRNA expression of Bcl10 and Map3k3 as determined by QPCR ($n = 3$ replicates per group). (K) Bar graphs showing relative total and phosphorylated TAK1 protein levels in *Tbc1d10c*^{+/+} and *Tbc1d10c*^{-/-} CD8 T cells from panel G ($n = 3$ replicates per group). P values were determined by unpaired Student's *t*-test.

The serine/threonine kinase Map3k3 is known to directly phosphorylate IKK complex members and mediate downstream NF- κ B activity.^{60,61} In untouched *Tbc1d10c*^{-/-} CD8 T cells, we observed a two-fold increase in Map3k3 protein (Figure 6G, I) that was not due to a change in *Map3k3* mRNA expression (Figure 6J). To investigate the relevance of this observation for CD8 T cell activation, we quantified Map3k3

protein levels following TCR ligation. Similar to untouched CD8 T cells, Map3k3 protein was increased two- to three-fold in *Tbc1d10c*^{-/-} CD8 T cells at 15, 30 and 60 min following TCR ligation (Figure 7A-B). These data suggest that i) *Tbc1d10c* activity negatively impacts Map3k3 protein stability and ii) *Tbc1d10c* may suppress canonical NF- κ B signaling by regulating Map3k3 protein levels. To address this idea, we performed

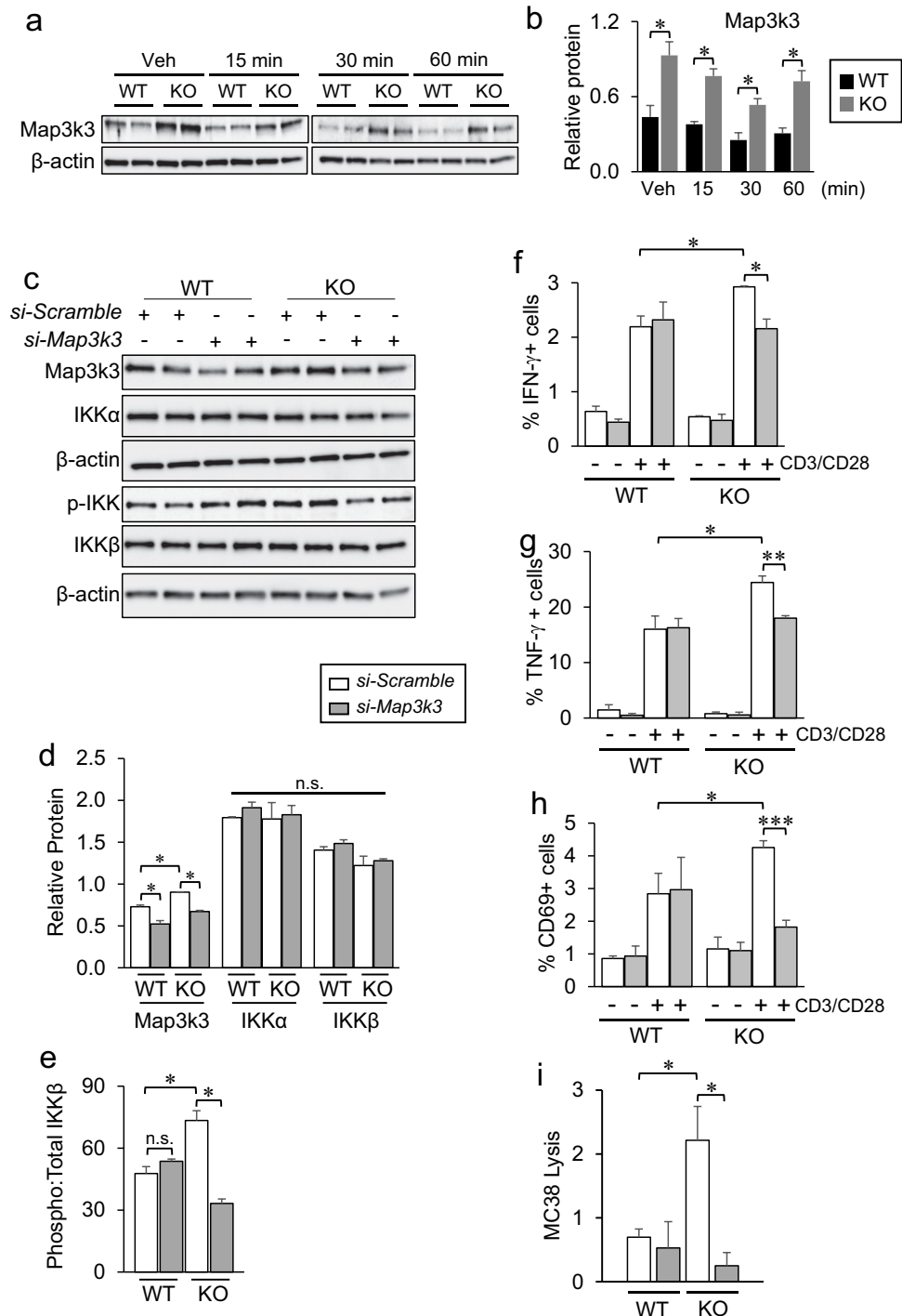


Figure 7. *Map3k3* knockdown rescues the *Tbc1d10c* null phenotype in CD8 T cells. (A-B) Gel images (A) and densitometric quantification (B) of total Map3k3 protein levels in *Tbc1d10c*^{+/+} and *Tbc1d10c*^{-/-} CD8 T cells following CD3/CD28 activation at the indicated time points ($n = 2$ replicates per group). (C-E) Gel images and densitometric quantification (bar graphs) showing relative total and phosphorylated protein levels of indicated proteins in Map3k3 siRNA knockdown *Tbc1d10c*^{-/-} CD8 T cells ($n = 2$ per replicates per group). (F-H) Percent of IFN- γ + (F), TNF- α + (G) and CD69+ (H) CD8 T cells following siRNA silencing of *Map3k3* and CD3/CD28 stimulation ($n = 3$ replicates per group). (I) Bar graph showing MC38 lysis levels by OT-I;*Tbc1d10c*^{+/+} and OT-I;*Tbc1d10c*^{-/-} CD8 T cells following *Map3k3* siRNA silencing at a 2:1 effector-to-target cell ratio ($n = 3$ per replicates per group). P values were determined by unpaired Student's *t*-test (*, $P < .05$; **, $P < .005$; ***, $P < .0005$).

siRNA knockdown of *Map3k3* and assessed its impact on activation levels of canonical NF- κ B pathway members known to be perturbed in *Tbc1d10c*^{-/-} CD8 T cells (Figure 5). *Map3k3* siRNA knockdown led to a two-fold decrease in the phosphorylation levels of IKK β protein with no impact on total protein levels of IKK α or IKK β in *Tbc1d10c*^{-/-} CD8 T cells (Figure 7C-E), indicating that the increased activation levels of canonical NF- κ B pathway members in *Tbc1d10c*^{-/-} CD8 T cells are Map3k3-dependent. Importantly, *Map3k3* siRNA knockdown rescued the activation and cytotoxic effector phenotype in *Tbc1d10c*^{-/-} CD8 T cells but had no effect on the activation or effector function of *Tbc1d10c*^{+/+} CD8 T cells (Figure 7F-I; Supplemental Figure S16A). Collectively, these observations support the conclusion that *Tbc1d10c* intersects the canonical NF- κ B pathway by negatively regulating Map3k3 protein levels and that Map3k3 is the key mediator of the *Tbc1d10c* null phenotype in CD8 T cells (Supplemental Figure S16B).

Discussion

We identified *Tbc1d10c* to be a selective and constitutive suppressor of CD8 T-cell activation and cytotoxic effector function. Mechanistically, our findings indicate that *Tbc1d10c* promotes tumor growth and incidence by tempering phosphorylation-dependent activation of IKK β via regulation of Map3k3 steady-state protein levels. While a tumor cell-specific role for *Tbc1d10c* is reported in large B cell lymphoma,⁶² our findings are the first to elaborate a cellular and molecular basis for *Tbc1d10c* signaling in solid malignancies. As such, our findings highlight the *Tbc1d10c*-Map3k3-NF- κ B signaling axis as a viable therapeutic target to promote anti-tumor immunity.

The NF- κ B pathway is a pleiotropic regulator of tumorigenesis.⁶³ In a variety of tumor cell types, the pro-tumorigenic effects of NF- κ B signaling are primarily levied during tumor promotion through enhancement of cancer cell proliferation and survival.⁶⁴ In addition to tumor cell-intrinsic mechanisms, NF- κ B signaling modulates the function of a variety of cellular constituents of the tumor microenvironment including macrophages, MDSCs, NK cells, lymphocytes, fibroblasts and endothelial cells.^{65,66} NF- κ B signaling also plays a role in T cell-mediated anti-tumor immunity. Canonical activation of NF- κ B in T cells increases the number of tumor-specific IFN- γ producing CD8 T cells and is required for tumor elimination.⁶⁷⁻⁶⁹ Collectively, this large body of published work underscores the importance and broad reach of the NF- κ B pathway in inflammation and cancer, while, in doing so, also implies the complexity associated with preventive or therapeutic approaches designed to block or activate NF- κ B signaling. In doing so, it stresses the importance of identifying NF- κ B pathway effectors or modifiers that discretely function in select immune lineages in their response to cancer.⁷⁰ Our findings show that *Tbc1d10c* blocks canonical NF- κ B (p65) transactivation downstream of TCR ligation in CD8 T cells but not in CD4 T cells. To our knowledge, there are no other published findings demonstrating discriminative mechanistic regulation of TCR-mediated canonical NF- κ B activation between CD4 and CD8 T-cell subsets as the downstream constituents of the

TCR pathways in each subset are largely thought to be analogous. A previous study in regulatory CD4 Tregs showed that selective inhibition of c-Rel, but not p65, blocked Treg immunosuppressive function and augmented the efficacy of PD-1 immune checkpoint inhibitor therapy while marginalizing cytotoxic side effects to normal tissue.⁷¹ However, conditional ablation of the non-canonical NF- κ B pathway component p100, a suppressor of RelB, in CD4 Tregs, manifests in RelB-mediated autoimmunity.⁷² While not involving *Tbc1d10c*, this work illustrated the impact of identifying and targeting T-cell subset-specific mechanisms that regulate NF- κ B activation on tumor outcome following immunotherapy.

Map3k3 regulates canonical NF- κ B pathway activation in T cells downstream of TCR ligation via direct phosphorylation of IKK β .^{60,61} Map3k3 expression knockdown completely rescued the *Tbc1d10c* null phenotype with respect to i) CD8 T cell activation and effector function and ii) NF- κ B pathway activation, indicating that *Tbc1d10c* intersects the NF- κ B pathway via Map3k3. As there is no precedence for interactions between these three proteins, our future work will focus on a potential role for *Tbc1d10c* GTPase function in the regulation of Map3k3 protein stability and the mechanistic basis for the discriminative interplay of these proteins in CD8 versus CD4 T cells.

Acknowledgments

We thank Charles Drake for the generous gift of B16-OVA cells and Wendy Mao for technical assistance with *in vitro* tumor cell killing assays. Pierre Chambon provided the *pCreER*^{T2} expression vector. Chyuan-Sheng Lin provided technical assistance with generation of *Tbc1d10c* null and *Tbc1d10c-CreER*^{T2} mice. We thank Ching-Yuan Chen, Caisheng Lu and Wei Wang for assistance with FACS sorting. We also thank Annemieke de Jong and Ioanna Karantza for assistance with isolating human CD8 T cells from whole blood. We are grateful to Donna Farber, Pawel Muranski and Arnold Han for their helpful advice on our study. The Genetically Modified Mouse Models, Genomics and High Throughput Screening, and Flow Cytometry Shared Resources within the HICCC are supported by NCI 5P30CA013696-44. Some Flow cytometry experiments were also performed in the CCTI Flow Cytometry Core, supported by NIH awards S10RR027050 and S10OD020056. A.O.C. was supported by NYDOH DOH01-C32582GG. S.H.W. was supported by NIH R01CA114014. J.C. and J. G. were supported by a Cancer Research Institute CLIP Award. R. D. and O.Y. were supported by NIH P30AR069632. M.A.B. was supported by NIH F32AR055007. D.M.O. was supported by a Cancer Research Institute CLIP Award, NIH P30AR069632 and NYDOH DOH01-C32582GG.

Disclosure statement

No potential conflict of interest was reported by the author(s).

Funding

The author(s) reported that there is no funding associated with the work featured in this article.

ORCID

David M. Owens  <http://orcid.org/0000-0003-0297-4370>

Author contributions

D.M.O. contributed to conceptualization; D.M.O., A.O.C., M.S.H., S.H.W., and M.A.B. contributed to methodology; A.O.C., J.Z., M.O.F., and R.K.S. contributed to formal analysis; A.O.C., S.H.W., J.Z., J.C., M.E.R., J.G., R.D., R.K.S., O.Y., D.Z.J., and M.A.B. contributed to investigation; A.O.C. and D.M.O. contributed to writing—original draft; A.O.C., J.Z. and D.M.O. contributed to writing—reviewing and editing; A.O.C., R.K.S. and D.M.O. contributed to visualization; D.M.O. contributed to supervision; D.M.O. contributed to funding acquisition.

References

- Waldman AD, Fritz JM, Lenardo MJ. A guide to cancer immunotherapy: from T cell basic science to clinical practice. *Nat Rev Immunol.* 2020;20(11):651–668. doi:10.1038/s41577-020-0306-5.
- Muenst S, Laubli H, Soysal SD, Zippelius A, Tzankov A, Hoeller S. The immune system and cancer evasion strategies: therapeutic concepts. *J Intern Med.* 2016;279(6):541–562. doi:10.1111/joim.12470.
- Mittal D, Gubin MM, Schreiber RD, Smyth MJ. New insights into cancer immunoediting and its component phases—elimination, equilibrium and escape. *Curr Opin Immunol.* 2014;27:16–25. doi:10.1016/j.coi.2014.01.004.
- Vinay DS, Ryan EP, Pawelec G, Talib WH, Stagg J, Elkord E, Lichtor T, Decker WK, Whelan RL, Kumara HMCS, et al. Immune evasion in cancer: mechanistic basis and therapeutic strategies. *Semin Cancer Biol.* 2015;35:S185–198. doi:10.1016/j.coi.2014.01.004.
- Pardoll DM. The blockade of immune checkpoints in cancer immunotherapy. *Nat Rev Cancer.* 2012;12:252–264. doi:10.1038/nrc3239.
- Giroux Leprieur E, Dumenil C, Julie C, Giraud V, Dumoulin J, Labrune S, Chinot T. Immunotherapy revolutionizes non-small-cell lung cancer therapy: results, perspectives and new challenges. *Eur J Cancer.* 2017;78:16–23. doi:10.1016/j.ejca.2016.12.041.
- Newick K, O'Brien S, Moon E, Albelda SM. CAR T cell therapy for solid tumors. *Annu Rev Med.* 2017;68(1):139–152. doi:10.1186/s13287-020-02128-1.
- Hopewell EL, Cox C, Pilon-Thomas S, Kelley LL. Tumor-infiltrating lymphocytes: streamlining a complex manufacturing process. *Cytotherapy.* 2019;21(3):307–314. doi:10.1016/j.jcyt.2018.11.004.
- Teply BA, Lipson EJ. Identification and management of toxicities from immune checkpoint-blocking drugs. *Oncology.* 2014;28(S3):30–38. PMID:25384885
- Kalaitidou M, Kueberuwa G, Schutt A, Gilham DE. CAR T-cell therapy: toxicity and the relevance to preclinical models. *Immunotherapy.* 2015;7(5):487–497. doi:10.2217/imt.14.123.
- Martins F, Sofiya L, Sykietis GP, Lamine F, Maillard M, Fraga M, Shabafrouz K, Ribic C, Cairoli A, Guex-Crosier Y, et al. Adverse effects of immune-checkpoint inhibitors: epidemiology, management and surveillance. *Nat Rev Clin Oncol.* 2019;16(9):563–580. doi:10.1038/s41571-019-0218-0.
- Wang DY, Salem JE, Cohen JV, Chandra S, Menzer C, Ye F, Zhao S, Das S, Beckermann KE, Ha L, et al. Fatal toxic effects associated with immune checkpoint inhibitors: a systematic review and meta-analysis. *JAMA Oncol.* 2018;4(12):1721–1728. doi:10.1001/jamaoncol.2018.3923.
- Eggermont AMM, Chiarion-Sileni V, Grob JJ, Dummer R, Wolchok JD, Schmidt H, Hamid O, Robert C, Ascierto PA, Richards JM, et al. Prolonged survival in stage III melanoma with ipilimumab adjuvant therapy. *N Engl J Med.* 2016;375(19):1845–1855. doi:10.1056/NEJMoa1611299.
- Weber JS, Kahler KC, Hauschild A. Management of immune-related adverse events and kinetics of response with ipilimumab. *J Clin Oncol.* 2012;30(21):2691–2697. doi:10.1200/JCO.2012.41.6750.
- Robert C, Long GV, Brady B, Dutriaux C, Maio M, Mortier L, Hassel JC, Rutkowski P, McNeil C, Kalinka-Warzocho E, et al. Nivolumab in previously untreated melanoma without BRAF mutation. *N Engl J Med.* 2015;372(4):320–330. doi:10.1056/NEJMoa1412082.
- Paz-Ares L, Luft A, Vicente D, Tafreshi A, Gumus M, Mazieres J, Hermes B, Cay Senler F, Csozsi T, Fulop A, et al. Pembrolizumab plus chemotherapy for squamous non-small-cell lung cancer. *N Engl J Med.* 2018;379(21):2040–2051. doi:10.1056/NEJMoa1810865.
- Khunger M, Rakshit S, Pasupuleti V, Hernandez AV, Mazzone P, Stevenson J, Pennell NA, Velcheti V. Incidence of pneumonitis with use of programmed death 1 and programmed death-ligand 1 inhibitors in non-small cell lung cancer: a systematic review and meta-analysis of trials. *Chest.* 2017;152(2):271–281. doi:10.1016/j.chest.2017.04.177.
- Postow MA, Chesney J, Pavlick AC, Robert C, Grossmann K, McDermott D, Linette GP, Meyer N, Giguere JK, Agarwala SS, et al. Nivolumab and ipilimumab versus ipilimumab in untreated melanoma. *N Engl J Med.* 2015;372(21):2006–2017. doi:10.1056/NEJMoa1414428.
- Kochenderfer JN, Somerville RPT, Lu T, Shi V, Bot A, Rossi J, Xue A, Goff SL, Yang JC, Sherry RM, et al. Lymphoma remissions caused by anti-CD19 chimeric antigen receptor T cells are associated with high serum interleukin-15 levels. *J Clin Oncol.* 2017;35(16):1803–1813. doi:10.1200/JCO.2016.71.3024.
- Davila ML, Riviere I, Wang X, Bartido S, Park J, Curran K, Chung SS, Stefanski J, Borquez-Ojeda O, Olszewska M, et al. Efficacy and toxicity management of 19-28z CAR T cell therapy in B cell acute lymphoblastic leukemia. *Sci Transl Med.* 2014;6(224):224ra25. doi:10.1126/scitranslmed.3008226.
- Brudno JN, Lam N, Vanasse D, Shen YW, Rose JJ, Rossi J, Xue A, Bot A, Scholler N, Mikkilineni L, et al. Safety and feasibility of anti-CD19 CAR T cells with fully human binding domains in patients with B-cell lymphoma. *Nat Med.* 2020;26(2):270–280. doi:10.1038/s41591-019-0737-3.
- Smith-Garvin JE, Koretzky GA, Jordan MS. T cell activation. *Annu Rev Immunol.* 2009;27(1):591–619. doi:10.1146/annurev.immu.02.1908.132706.
- Garcia E, Ismail S. Spatiotemporal regulation of signaling: focus on T cell activation and the immunological synapse. *Int J Mol Sci.* 2020;21(9):3283. doi:10.3390/ijms21093283.
- Hwang JR, Byeon Y, Kim D, Park SG. Recent insights of T cell receptor-mediated signaling pathways for T cell activation and development. *Exp Mol Med.* 2020;52(5):750–761. doi:10.1038/s12276-020-0435-8.
- Pan F, Sun L, Kardian DB, Whartenby KA, Pardoll DM, Liu JO. Feedback inhibition of Calcineurin and Ras by a dual inhibitory protein Carabin. *Nature.* 2007;445(7126):433–436. doi:10.1038/nature05476.
- Schickel JN, Pasquali JL, Soley A, Knapp AM, Decossas M, Kern A, Fauny JD, Marcellin L, Korganow AS, Martin T, et al. Carabin deficiency in B cells increases BCR-TLR9 costimulation-induced autoimmunity. *EMBO Mol Med.* 2012;4(12):1261–1275. doi:10.1002/emmm.201201595.
- Song Y, Pan Y, Liu J. The relevance between the immune response-related gene module and clinical traits in head and neck squamous cell carcinoma. *Cancer Manag Res.* 2019;11(21):7455–7472. doi:10.2147/CMAR.S201177.
- Zeng H, Song X, Ji J, Chen L, Liao Q, Ma X. HPV infection related immune infiltration gene associated therapeutic strategy and clinical outcome in HNSCC. *BMC Cancer.* 2020;20(1):796. doi:10.1186/s12885-020-07298-y.
- Tang L, Peng C, Zhu SS, Zhou Z, Liu H, Cheng Q, Chen X, Chen X-P. Tre2-Bub2-Cdc16 family proteins based nomogram serve as a promising prognosis predicting model for melanoma. *Front Oncol.* 2020;10:579625. doi:10.3389/fonc.2020.579625.
- Bai F, Jin Y, Zhang P, Chen H, Fu Y, Zhang M, Weng Z, Wu K. Bioinformatic profiling of prognosis-related genes in the breast cancer immune microenvironment. *Aging (Albany NY).* 2019;11:9328–9347. doi:10.18632/aging.102373.

31. Choy CT, Wong CH, Chan SL. Embedding of genes using cancer gene expression data: biological relevance and potential application on biomarker discovery. *Front Genet.* 2019;9:682. doi:10.3389/fgene.2018.00682.
32. Liu P, Jenkins NA, Copeland NG. A highly efficient recombining-based method for generating conditional knock-out mutation. *Genome Res.* 2003;13(3):476–484. doi:10.1101/gr.749203.
33. Muzumdar MD, Tasic B, Miyamichi K, Li L, Luo L. A global double-fluorescent Cre reporter mouse. *Genesis.* 2007;45(9):593–605. doi:10.1002/dvg.20335.
34. Hao H, Rajewsky K. Homeostasis of peripheral B cells in the absence of B cell influx from the bone marrow. *J Exp Med.* 2001;194(8):1151–1164. doi:10.1084/jem.194.8.1151.
35. Hogquist KA, Jameson SC, Heath WR, Howard JL, Bevan MJ, Carbone FR. T cell receptor antagonist peptides induce positive selection. *Cell.* 1994;76(1):17–27. doi:10.1016/0092-8674(94)90169-4.
36. Barnden MJ, Allison J, Heath WR, Carbone FR. Defective TCR expression in transgenic mice constructed using cDNA-based alpha- and beta- chain genes under the control of heterologous regulatory elements. *Immunol Cell Biol.* 1998;76(1):34–40. doi:10.1046/j.1440-1711.1998.00709.x.
37. Stumpfova M, Ratner D, Desciak EB, Eliezri YD, Owens DM. The immunosuppressive surface ligand CD200 augments the metastatic capacity of squamous cell carcinoma. *Cancer Res.* 2010;70(7):2962–2972. doi:10.1158/0008-5472.CAN-09-4380.
38. Bellone M, Cantarella D, Castiglioni P, Crosti MC, Ronchetti A, Moro M, Garancini MP, Casorati G, Dellabona P. Relevance of the tumor antigen in the validation of three vaccination strategies for melanoma. *J Immunol.* 2000;165(5):2651–2656. doi:10.4049/jimmunol.165.5.2651.
39. Toews GB, Bergstresser PR, Streilein JW. Epidermal Langerhans cell density determines whether contact hypersensitivity or unresponsiveness follows skin painting with DNFB. *J Immunol.* 1980;124(1):445–453. PMID:6153101
40. Curran MA, Montalvo W, Yagita H, Allison JP. PD-1 and CTLA-4 combination blockade expands infiltrating T cells and reduces regulatory T and myeloid cells within B16 melanoma tumors. *Proc Natl Acad Sci USA.* 2010;107(9):4275–4280. doi:10.1073/pnas.0915174107.
41. Khan IZ, Del Guzzo CA, Shao A, Cho J, Du R, Cohen AO, Owens DM. The CD200-CD200R axis promotes squamous cell carcinoma metastasis via regulation of cathepsin K. *Cancer Res.* 2021;81(19):5021–5032. doi:10.1158/0008-5472.CAN-20-3251.
42. Rheinwald JG, Green H. Serial cultivation of strains of human epidermal keratinocytes: the formation of keratinizing colonies from single cells. *Cell.* 1975;6(3):331–343. doi:10.1016/s0092-8674(75)80001-8.
43. Yang Y, Xiang Z, Ertl HC, Wilson JM. Upregulation of class I major histocompatibility complex antigens by interferon gamma is necessary for T-cell-mediated elimination of recombinant adenovirus-infected hepatocytes in vivo. *Proc Natl Acad Sci USA.* 1995;92(16):7257–7261. doi:10.1073/pnas.92.16.7257.
44. Zheng GX, Terry JM, Belgrader P, Ryykin P, Bent ZW, Wilson R, Ziraldo SB, Wheeler TD, McDermott GP, Zhu J, et al. Massively parallel digital transcriptional profiling of single cells. *Nat Commun.* 2017;8(1):14049. doi:10.1038/ncomms14049.
45. Hao Y, Hao S, Andersen-Nissen E, Mauck WM, Zheng S, Butler A, Lee MJ, Wilk AJ, Darby C, Zager M, et al. Integrated analysis of multimodal single-cell data. *Cell.* 2021;184(13):3573–3587. doi:10.1016/j.cell.2021.04.048.
46. Andreatta M, Corria-Osorio J, Müller S, Cubas R, Coukos G, Carmona SJ. Interpretation of T cell states from single-cell transcriptomics data using reference atlases. *Nat Commun.* 2021;12(1):2965. doi:10.1038/s41467-021-23324-4.
47. Bruderer R, Bernhard OM, Gandhi T, Miladinovic SM, Cheng LY, Messner S, Ehrenberger T, Zanutelli V, Butscheid Y, Escher C, et al. Extending the limits of quantitative proteome profiling with data-independent acquisition and application to Acetaminophen-treated three-dimensional liver microtissues. *Mol Cell Proteomics.* 2015;14(5):1400–1410. doi:10.1074/mcp.M114.044305.
48. Kulak NA, Pichler G, Paron I, Nagaraj N, Mann M. Minimal, encapsulated proteomic-sample processing applied to copy-number estimation in eukaryotic cells. *Nat Methods.* 2014;11(3):319–324. doi:10.1038/nmeth.2834.
49. Bachelor MA, Lu Y, Owens DM. L-3-Phosphoserine phosphatase (PSPH) regulates cutaneous squamous cell carcinoma proliferation independent of L-serine biosynthesis. *J Dermatol Sci.* 2011;63:164–1672. doi:10.1016/j.jdermsci.2011.06.001.
50. Feil R, Wagner J, Metzger D, Chambon P. Regulation of Cre recombinase activity by mutated estrogen receptor ligand-binding domains. *Biochem Biophys Res Comm.* 1997;237(3):752–757. doi:10.1006/bbrc.1997.7124.
51. Campanella GSV, Luster AD. Chapter 18. A chemokine-mediated in vivo T-cell recruitment assay. *Methods Enzymol.* 2009;461:397–412. doi:10.1016/S0076-6879(09)05418-4.
52. Li T, Lu H, Shen C, Lahiri SK, Wason MS, Mukherjee D, Yu L, Zhao J. Identification of epithelial stromal interaction 1 as a novel effector downstream of Krüppel-like factor 8 in breast cancer invasion and metastasis. *Oncogene.* 2013;33(39):4746–4755. doi:10.1038/onc.2013.415.
53. Ghosh S, Baltimore D. Activation in vitro of NF-kappa B by phosphorylation of its inhibitor I kappa B. *Nature.* 1990;344(6267):678–682. doi:10.1038/344678a0.
54. Schulze-Luehrmann J, Ghosh S. Antigen-receptor signaling to nuclear factor κ B. *Immunity.* 2006;25(5):701–715. doi:10.1016/j.immuni.2006.10.010.
55. Isakov N, Altman A. PKC-theta mediated signal delivery from the TCR/CD28 surface receptors. *Front Immunol.* 2012;3:273. doi:10.3389/fimmu.2012.00273.
56. Gehring T, Seeholzer T, Krappmann D. Bcl10 – bridging CARDs to immune activation. *Front Immunol.* 2018;9:1539. doi:10.3389/fimmu.2018.01539.
57. Zhou H, Wertz I, O'Rourke K, Ultsch M, Seshagiri S, Eby M, Xiao W, Dixit VM. Bcl10 activates the NF-kappaB pathway through ubiquitination of NEMO. *Nature.* 2004;427(6970):167–171. doi:10.1038/nature02273.
58. Stelzer G, Rosen R, Plaschkes I, Zimmerman S, Twik M, Fishilevich S, Stein TI, Nudel R, Lieder I, Mazor Y, et al. The GeneCards Suite: from Gene Data Mining to Disease Genome Sequence Analysis. *Curr Protoc Bioinformatics.* 2016;54(1):1.30.1–1.30.33. doi:10.1002/cpbi.5.
59. Becnel LB, Ochsner SA, Darlington YF, McOwiti A, Kankanamge WH, Dehart M, Naumov A, McKenna NJ. Discovering relationships between nuclear receptor signaling pathways, genes and tissues in Transcriptome. *Sci Signal.* 2017;10(476):eaah6275. doi:10.1126/scisignal.aah6275.
60. Di Y, Li S, Wang L, Zhang Y, Dorf ME. Homeostatic interactions between MEKK3 and TAK1 involved in NF- κ B signaling. *Cell Signal.* 2008;20(4):705–713. doi:10.1016/j.cellsig.2007.12.007.
61. Samanta AK, Huang HJ, Bast RC, Liao WSL. Overexpression of MEKK3 confers resistance to apoptosis through activation of NFkappaB. *J Biol Chem.* 2004;279(9):7576–7583. doi:10.1074/jbc.M311659200.
62. Jiang W, Zhou X, Li Z, Liu K, Wang W, Tan R, Cong X, Shan J, Zhan Y, Cui Z, et al. Prolyl 4-hydroxylase 2 promotes B-cell lymphoma progression via hydroxylation of Carabin. *Blood.* 2018;131(12):1325–1336. doi:10.1182/blood-2017-07-794875.
63. Taniguchi K, Karin M. NF- κ B, inflammation, immunity and cancer: coming of age. *Nat Rev Immunol.* 2018;18(5):309–324. doi:10.1038/nri.2017.142.
64. Karin M, Greten FR. NF- κ B: linking inflammation and immunity to cancer development and progression. *Nat Rev Immunol.* 2005;5(10):749–759. doi:10.1038/nri1703.
65. Grivennikov SI, Greten FR, Karin M. Immunity, inflammation, and cancer. *Cell.* 2010;140(6):883–899. doi:10.1016/j.cell.2010.01.025.

66. Quail DF, Joyce JA. Microenvironmental regulation of tumor progression and metastasis. *Nat Med.* 2013;19(11):1423–1437. doi:10.1038/nm.3394.
67. Gerondakis S, Siebenlist U. Roles of NF- κ B pathway in lymphocyte development and function. *Cold Spring Harb Perspect Biol.* 2010;2(5):a000182. doi:10.1101/cshperspect.a000182.
68. Gerondakis S, Fulford TS, Messina NL, Grumont RJ. NF- κ B control of T cell development. *Nat Immunol.* 2014;15(1):15–25. doi:10.1038/ni.2785.
69. Evaristo C, Spranger S, Barnes SE, Miller ML, Molinero LL, Locke FL, Gajewski TF, Alegre ML. Cutting edge: engineering active IKK α in T cells drives tumor rejection. *J Immunol.* 2016;196(7):2933–2938. doi:10.4049/jimmunol.1501144.
70. Mortezaee K, Najafi M, Farhood B, Ahmadi A, Shabeeb D, Musa AE. NF- κ B targeting for overcoming tumor resistance and normal tissues toxicity. *J Cell Physiol.* 2019;234(10):17187–17204. doi:10.1002/jcp.28504.
71. Grinberg-Bleyer Y, Oh H, Desrichard A, Bhatt DM, Caron R, Chan TA, Schmid RM, Klein U, Hayden MS, Ghosh S. NF- κ B c-Rel is crucial for the regulatory T cell immune checkpoint in cancer. *Cell.* 2017;170(6):1096–1108. doi:10.1016/j.cell.2017.08.004.
72. Grinberg-Bleyer Y, Caron R, Seeley JJ, De Silva NS, Schindler CW, Hayden MS, Klein U, Ghosh S. The alternative NF- κ B pathway in regulatory T cell homeostasis and suppressive function. *J Immunol.* 2018;200(7):2362–2371. doi:10.4049/jimmunol.1800042.